CHALMERS
UNIVERSITY OF TECHNOLOGY

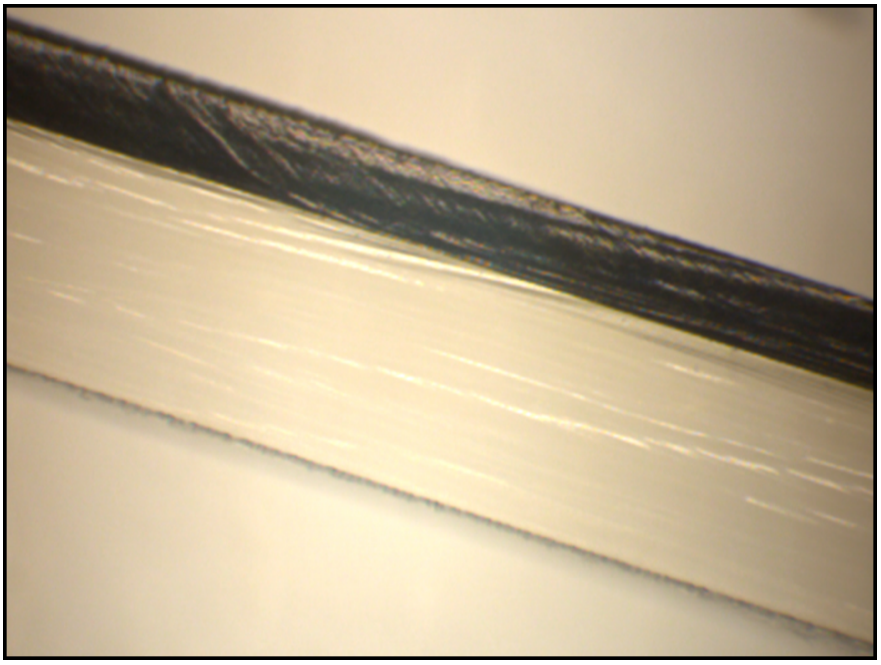

Electric conductivity measurements including the semiconductor-insulator interface from HVDC cables

Master's thesis in Electric Power Engineering

ÖRJAN HAGBERG
CARL WAGNÉ

Department of Electrical Engineering
CHALMERS UNIVERSITY OF TECHNOLOGY
Gothenburg, Sweden 2019

Master's thesis

Electric conductivity measurements including the semiconductor-insulator interface from HVDC cables

Örjan Hagberg
Carl Wagné

CHALMERS
UNIVERSITY OF TECHNOLOGY

Electric Power Engineering
Department of Electrical Engineering
Chalmers University of Technology
Gothenburg, Sweden 2019

Electric conductivity measurements including the semiconductor-insulator interface from HVDC cables.
Örjan Hagberg
Carl Wagné

Supervisors:
Espen H. Doedens, Nexans AS NO-1751 Halden, Norway
Markus Jarvid, Nexans AS NO-1751 Halden, Norway
Xiangdong Xu, Department of Electrical Engineering
Examiner: Prof. Yuriy Serdyuk, Department of Electrical Engineering

Master's Thesis
Department of Electrical Engineering
Chalmers University of Technology
SE-412 96 Gothenburg
Telephone +46 31 772 1000

Cover: Microscope image of a cable peeling sample.

Typeset in LaTeX
Gothenburg, Sweden 2019

"Kill the boy, and let the man be born."
-Aemon Targaryen

Abstract

As global power consumption increases along with increased demands for renewable energy, additional expansions of the existing power grids are required. Extruded HVDC cable systems can be a potent solution to this power transmission problem, both because of its technological advantages allowing for full power flow control as well as its effectiveness compared to HVAC in transporting power over long distances. To ensure reliability and long life time of the extruded HVDC cables, it is of paramount importance to understand fully their characteristics. For this, full scale testing of produced HVDC cables can be performed, but it is time consuming and expensive. Alternatively, small scale testing can be realized on samples of the cable.

The purpose of this master thesis was to develop a test set-up for small scale testing of cable insulation and to determine the electrical conductivity of insulation material using two types of samples, namely, cable peelings containing insulation-semiconductor interfaces and press-molded plates with comparable geometry. In addition, optical profilometry and microscope studies were conducted along with temperature cycling test to investigate the chosen press-film for the press-molded plates.

The performed studies are presented in the report. The test set up was constructed and validated by comparing the measurement results with available data from literature. Furthermore, conductivity measurements were performed with two types of samples for three electric field levels and two different temperatures (30°C and 70°C). The acquired results were found in a plausible range and were used to identify differences in the conductivities of cable peelings and press-moulded plates. These samples were further analysed with optical profilometry, which indicated no significant differences in surface texture and roughness between the two different sample types. From the temperature cycling test, it was concluded that the chosen press-film had no effect on non-monotonic conductivity of the press-molded samples. The performed study broadened understanding of properties of semiconductor-insulation interfaces of HVDC cables.

Keywords: HVDC, XLPE, cable peeling, press-moulded plate, leakage current, conductivity, roughness, charge injection.

Sammanfattning

Eftersom den globala energiförbrukningen ökar tillsammans med en högre efterfrågan på förnybar energi krävs ytterligare utvidgningar av befintliga elnät. Extruderade HVDC-kabelsystem kan vara en lämplig lösning på detta kraftöverföringsproblem, både på grund av dess tekniska fördelar, vilket möjliggör fullständig styrning av effektflödet, och dess effektivitet jämfört med HVAC vid transport av kraft över långa avstånd. Det är emellertid av största vikt att egenskaperna hos de extruderade HVDC-kablarna förstås fullt så att konstruktionen är pålitlig och en lång livslängd kan säkerställas. Att utföra test i full skala av producerade HVDC-kablar är tidskrävande och dyrt, vilket kan undvikas genom småskaliga tester som utförs på specifika prover av kabeln. I detta examensarbete ligger fokus på kabelns isolations-halvledargränssnitt och därför extraherades kabelskalningar innehållande detta gränssnitt.

Syftet var att utveckla en testuppsättning för småskaliga tester och för att bestämma den elektriska ledningsförmågan hos sådana kabelskalningar och även för pressgjutna plattor med jämförbar geometri. Vidare är det av intresse att diskutera om det finns någon skillnad mellan de två provtyperna. Elektrisk ledningsförmåga är beroende av flera olika fenomen, vilket leder till behovet av icke-elektriska tester; optiska profilometri och mikroskopstudier, tillsammans med ett temperaturcykeltest för att undersöka effekten av den valda pressfilmen för de pressgjutna plattorna. Detta gav en bred förståelse, vilket i sin tur leder till mer tillförlitlig analys av den uppmätta ledningsförmågan. Från temperaturcykeln drogs slutsatsen att den valda pressfilmen gav transientfria konduktivitetsvariationer hos de pressgjutna proven. Den optiska profilometrin gav också resultat som indikerar att det inte finns en signifikant skillnad i ytjämnhet mellan de två olika proven. Den konstruerade testuppsättningen fungerade som förväntat, och i jämförelse med andra studier drogs slutsatsen att den uppmätta konduktiviteten från de skalade proven var rimlig.

Acknowledgements

First of all we would like to give our appreciation to Nexans Norway AS for giving us this opportunity. Extra appreciation goes to the employees of Nexans that have helped us during the master thesis, these are; Heine Pettersen, Jan-Are Sundby and Ole Løkkeberg. Special gratitude to Xiangdong Xu for his experience and expertise with conductivity measurements, which he happily shared with us. Particularly we would like to thank him for his practical knowledge and support when we struggled with our measurements. Especially we would like to thank Yuriy Serdyuk for accepting to be the thesis examiner. Nevertheless, we would like to thank Örjans parents for lending us their car which made it possible for us to easily travel back and forth to Norway. Gratitude is expressed to Arvid Björemark for his help with our measurements when we were on conference. Another thanks to Johan Ivarsson and Per Wiklund for their consulting and cheerful endeavours in times when a laughter was needed. Markus Jarvid is further acknowledged for the interesting discussions and information he provided regarding polyethylene. Most of all, we would like to thank Espen Doedens for being not only a dedicated and helpful supervisor, but also a good friend and a role model during the entirety of the master thesis. Admittedly, this thesis would not be possible without him, and he has our deepest gratitude.

Örjan Hagberg & Carl Wagné, Gothenburg, June 2019

Contents

List of Figures **xiii**

List of Tables **xvii**

1 Introduction **1**
1.1 Background . . . 1
1.2 Aim . . . 2
1.3 Scope . . . 2
1.4 Methodology . . . 2
1.5 Societal, ethical and ecological aspects . . . 3
1.5.1 Societal . . . 4
1.5.2 Ethical . . . 4
1.5.3 Ecological . . . 4

2 Theory **5**
2.1 HVDC-cable . . . 5
2.1.1 Insulation . . . 7
2.1.2 Semi-conductor . . . 11
2.2 Electric conductivity of insulating polymers . . . 12
2.2.1 Energy band theory and its application to polymers . . . 12
2.2.2 Electronic conduction within the insulation . . . 14
2.2.3 Macroscopic conductivity expression . . . 16
2.2.4 Reduction of impurity content . . . 16
2.2.5 Charge injection on metal-polymer interfaces . . . 17
2.2.5.1 Surface roughness . . . 19

3 Methods **21**
3.1 Test samples . . . 21
3.1.1 Cable peelings . . . 21
3.1.2 Press-molded plates . . . 22
3.1.3 Optical profilometry . . . 23
3.2 Test set-up . . . 24
3.2.1 Test-set up TC1, TC1-G, TC2 . . . 24
3.2.2 Test-cell TC1 and TC1-G . . . 25
3.2.3 Test-cell TC2 . . . 26
3.2.4 Safety measures for the test set-ups . . . 26
3.2.5 Pressure calibration . . . 27

3.2.6 High voltage circuit 28
3.2.7 Measurements of the current 30
3.2.8 LabView-program 30
3.3 Testing 32

4 Results **33**
4.1 Kapton as film for press-molded plates 33
4.2 Roughness measurements 34
4.3 Cable peeling- and press-molded plate thickness 37
4.4 Benchmarking of test-cells 38
4.5 Results of conductivity measurements 42
4.5.1 Cable peelings 42
4.5.2 Press-molded plates 44

5 Conclusion **47**
5.1 Discussion 47
5.2 Conclusion 53

6 Future work **55**
6.1 Roughness measurements 55
6.2 Noise levels 55
6.3 Byproduct measurement 56
6.4 Cable peelings and press-molded plates 56

Bibliography **57**

A Appendix I **I**

List of Figures

1.1 A principle sketch of the test set-up for the leakage current measurement. . . . 3

2.1 Description of the layers in a typical extruded submarine HVDC-cable. 5
2.2 Shape of the polyethylene molecule depending on polymerisation process. a) HDPE, b) LDPE and c) XLPE 9
2.3 The growth of spherulites in a material. Straight lines indicate lamellae (not to scale). . . . 10
2.4 The process of converting a semi-crystalline polymer from more being randomly oriented to more non-randomly oriented, during mechanical stress or cable extrusion. . . . 11
2.5 A simple illustration of how energy bands and band gaps are formed. 13
2.6 The extended model of the energy band (E_g) for polyethylene. (a) A more realistic representation of the energy band with the impact of states and traps. (b) Description of the new energy states in turns of trap-density. (c) The modelled energy states included in the energy band. . . . 14
2.7 (a) The level of the energy band for the different interfaces in the test cell.(b) The energy band model implemented on the semicon-insulation interface. The ground electrode is not shown. . . . 17
2.8 (a) The energy band of the metal-insulator interface during the impact of electric field. (b) The extended model for the field lowering effect of the Schottky barrier on the metal-insulation interface. . . . 18

3.1 The process for the press-molded "sandwich". (a) The procedure for the insulation and semiconductor plates. (b) The construction of the finalised plate, where the separate plates are pressed together and crosslinked. . . . 23
3.2 Simple schematic of how the TC1-G is connected and what instruments are used. . . . 24
3.3 The TC1-G and its different key components. . . . 25
3.4 Illustration of the necessary parts of TC2. . . . 26
3.5 The pressure experienced by the sample within the test cell per rotations of the bolts. . . . 27
3.6 In-detail schematic of how the Glassman high voltage power supply is controlled. . . . 28
3.7 Overview of the ADAM-4022T device and its different ports. . . . 28

3.8 Back-side of the Glassman power supply and its different connection points. 29
3.9 This is the graphical user interface of the LabView-program used to control the instruments and acquire data. 31

4.1 Results from temperature cycling test with a press-molded plate manufactured with kapton as press-film, where the temperature cure is an indication of temperature set points and not the actual internal sample temperature. 33
4.2 Insulation surface scan of a) peeled sample and b) press-molded sample. 34
4.3 Surface height histogram indicating the deviation from the mean height of the surface. 35
4.4 Box plot for the S_a parameter for the different interfaces where backside refers to the cable peelings, kapton molded ins and sc to the insulation and semiconductive side of the press-molded plates respectively. 36
4.5 Box plot for the S_q parameter for the different interfaces where backside refers to the cable peelings, kapton molded ins and sc to the insulation and semiconductive side of the press-molded plates respectively. 36
4.6 One of the cross-sections from the microscopy used to determine the insulation thickness of sample O14. 37
4.7 Leakage current measurement of insulation cable peeling using; (a) TC1, (b) TC2 and (c) TC1-G at three different poling voltages. . . . 38
4.8 Leakage current measurement of semiconductor-insulation cable peeling using; (a) TC1, (b) TC2 and (c) TC1-G. 40
4.9 Effect of the DC capacitor on the leakage current measurement using TC2. 41
4.10 Measurement data for peeled sample O08 during 70°C with test-cell TC1 at voltage levels 3.7, 7.4 and 11 kV. 42
4.11 One data point from each field level for the cable peelings is plotted and the lines represent an exponential fit of the data points. 43
4.12 Measurement data for press-molded plate #1 during 70°C with test-cell TC1 at voltage levels 3.7, 7.4 and 11 kV. 44
4.13 One data point from each field level for the press-molded plates is plotted and the lines represent the fit of the conductivity equation to the data points. 45

5.1 The three different test-cells with the triple point marked as a red dot. 48
5.2 TC1-G and TC1 with the equipotential lines and the electric field distribution. 48
5.3 Example of noisy measurement using TC2 for a longer measurement at voltage 2.5, 5 and 7.5 kV. 49

A.1 Thickness of three different samples from cable peeling O08. I
A.2 Thickness of three different samples from cable peeling O10. II

A.3 Thickness of three different samples from cable peeling O11. II
A.4 Thickness of three different samples from cable peeling O14. III
A.5 Thickness of two different samples from cable peeling O15. III

List of Tables

4.1 S_a, S_q and S_{dq} parameters for the different samples presented in Figure 4.3 35
4.2 All the samples and their respective average thickness, as well as the different electric field depending on the three different voltage levels. . 38
4.3 Measurement values of current and conductivity for the peeled samples after 12 hours. 43
4.4 Measurement values of current and conductivity for the press-molded samples after 12 hours. 44
4.5 The values of α, β and σ_0 for each sample. 45

1
Introduction

With a flourishing society, urban energy demand as well as further electrification of heating and transport sectors increases by the day. Additionally, there is an environmental mindset where the CO_2 emissions and fossil fuel usage needs to be reduced in order to minimise negative impact on our future generations. This demands new and more sustainable energy production and transmission solutions. Renewable energy sources combined with electrical grid expansion, connecting larger areas, is commonly considered as a solution to mitigate these increasing emissions. This creates a high demand for high voltage cables and facilitates a continued research effort for improving transmission systems and increasing to ever higher voltage levels. Submarine HVDC links could be a potent solution to overcome these future problems. During the last couple of years there has been an immense progress within the extruded HVDC cable technology that utilises polyethylene (XLPE) as its insulation system and is of today a strong competitor to traditional mass impregnate (MI) insulation system. Benefits, such as higher rated operating temperature and a faster assembly process for its accessories, have led to development of higher power ratings of produced XLPE cables. Even though there is deep knowledge of polyethylene cables today, there are still some characteristics of the cable, such as the semiconductor - insulation interface, that are not yet fully understood. This interface is present in all extruded high voltage cables, and for the development of HVDC transmission systems there is particular need to further understand the nature and relevant parameters of this interface.

1.1 Background

An HVDC extruded cable consists of several different layers, e.g. conductor, inner semiconductive layer, cable insulation and outer semiconductive screen [1]. When performing an installation of an HVDC cable system there will additionally be need for joints and terminations. These accessories will in turn introduce additional material interfaces, which may cause vulnerable points [2]. The result of poor design of such interfaces might be a shorter life span of the HVDC cable system. Of course this must be avoided by all means since a long life span and high reliability is demanded by the customers for an HVDC cable system [2].

It is of great importance to understand and study these interfaces, and the most commonly used method is creating press-molded plates. Such plates however, might not replicate exactly the chemical and physical nature of the interface created in the

HV cable manufacturing process. Press-molded plates can be, insulation and semiconductor material pressed together during high pressure and temperature such that the plate becomes cross-linked. The result is a sample of the cable materials that can be electrically tested. Recently an alternative to create and test press-molded plates have been utilised at Nexans Norway. Instead of pressing the cable-material together during high pressure a cable peeling is cut out from a full-size cable, close to the outer semi-conductive layer, and is then electrically tested in the exact same manner as the press-molded plate. This cable peeling thus features identical chemo-physical characteristics of the internal interface compared to the HV cable. Example of electrical measurements that can be performed on cable peelings or press-molded plates are, for example; conductivity measurements, Direct Current Breakdown (DCBD) and charge decay. By performing such measurements on cable peelings an understanding of the behaviour of semiconductor - insulation interfaces can be acquired.

1.2 Aim

The aim of this master thesis is to develop and construct a leakage current testing set-up for the investigation of the semiconductor-insulation interface of an HVDC cable. This allows us to see if there is a difference in conductivity of a cable peeling compared to a press-molded sample with identical material and similiar geometry at different electric field levels and temperatures.

1.3 Scope

During this project there was only one interface that was examined, the (outer) semiconductor - insulation interface.

The focus of the project was on the electrical behaviour of the semiconductor - insulation interface, however since the chemo-physical nature of the polymer interfaces are of great importance for the end results of the conductivity measurements, some material characterisations were performed.

1.4 Methodology

The project started at Chalmers University of Technology where a test set-up for the leakage current measurement was created. The set-up presented in Figure 1.1 is an overview of the testing circuit. The explanations of the different "objects" illustrated in Figure 1.1 are presented below:

- The Glassman high voltage DC supply (50 kV) was used to provide a sufficiently high DC voltage to the high voltage electrode of the test-cell.
- The test-cell was designed by one of the project Supervisors, Espen Doedens. Its purpose is to apply high voltage to the semiconductive side of the samples and measure the current with help of an electrometer. The test-cell is further explained in section 3.2.2.

- A protection box, was placed in between the electrometer and the test cell. This was used in order to protect the electrometer.
- A Keithley 6517B Electrometer was used to measure the leakage current of the sample. It has a current measuring range of ± 10 [aA] to ± 21 [mA] [3].

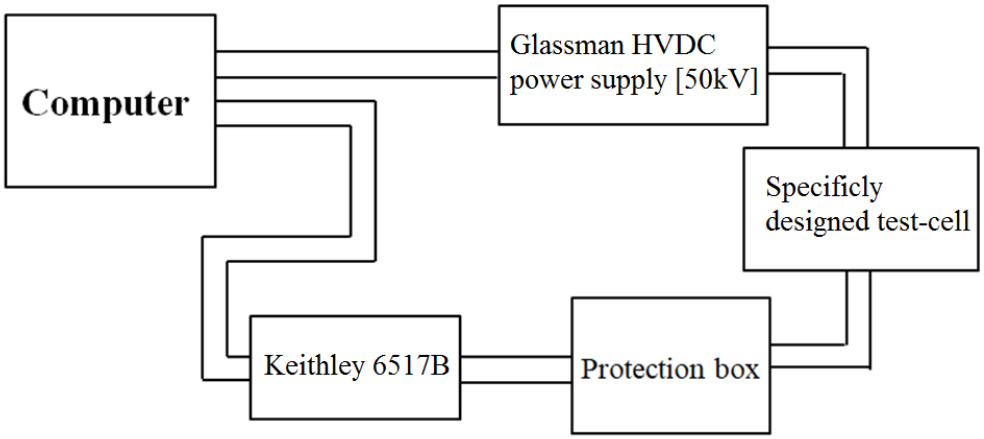

Figure 1.1: A principle sketch of the test set-up for the leakage current measurement.

In parallel with the creation of the set-up a comprehensive literature study was performed, which provided useful knowledge regarding leakage current testing, HVDC-cables and its materials, as well as conductivity. The test-cell was designed from scratch and custom fabricated, since there were no existing ones available. In order to successfully control the voltage source and to conduct the measurements, dedicated software was developed.

Besides creating the measurement set-up a sufficient amount of cable peelings and press-molded plates was produced. These samples were produced at the Material lab of Nexans Norway, with the help from the employees of the lab.

Once the set-up was completed and sufficienly accurate and satisfying results were achieved (with regards of noise and reasonable behaviour) the test-cell was put into a heating chamber at Chalmers University of Technology, where all the final results could be acquired during controlled temperature conditions.

1.5 Societal, ethical and ecological aspects

In this section some thoughts will be presented regarding the societal, ethical and ecological aspects of this project. It is important in today's society that these aspects are taken into regard when performing new engineering projects, to justify the significance of the project.

1.5.1 Societal

Electricity is a key factor for maintaining both living standards, but additionally supplying clean energy sources to today's society. A vast majority of the population in the world is somewhat dependent on a reliable supply of electricity. As mentioned in section 1.1, reliability and a long life span of the cable are demanded by the customers. Increasing the understanding of the material interfaces could positively affect both the reliability and the life span, which in a societal aspect clearly justifies the execution of this master thesis by increasing the standard of living for people all around the world.

1.5.2 Ethical

The ethical point of view in this case is similar to that of the societal view. It can be argued that a more reliable cable system will also provide an increased quality of life for the majority of the population. Additionally, higher quality cables could compete better with overhead lines, providing less negative impact on nearby habitants to the transmission line.

1.5.3 Ecological

With more renewable energy source introduced to the power system reliability and life time expectancy of the transmission system needs to be improved. Since the renewable energy sources often are located off-shore there will be more focus on longer submarine cables. In order to follow the development and ensure a longer life time of the cables, uncertainties needs to be investigated. Since this project focuses on increasing the knowledge of the functionally and in turn could increase the life time expectancy, our project will have significant value from an ecological aspect.

2

Theory

A comprehensive literature study has been performed and the relevant theory for this master thesis is presented in this chapter. The two main parts are section 2.1 and 2.2, which are ”HVDC-cable” and ”Electric conductivity of insulating polymers” respectively. In the former, theory regarding the insulation and the semiconductor of the cable is given and in the latter information regarding the concept of conductivity and how it applies to the insulation is presented.

2.1 HVDC-cable

In this section the main parts of a typical submarine HVDC cable together with the manufacturing process, of importance for this project, will be explained. Worth mentioning is that all high voltage cables are customly manufactured for specific applications and conditions, which means that the produced cables are unique and separate from one another. In Figure 2.1 the cross section of a typical submarine HVDC cable is depicted.

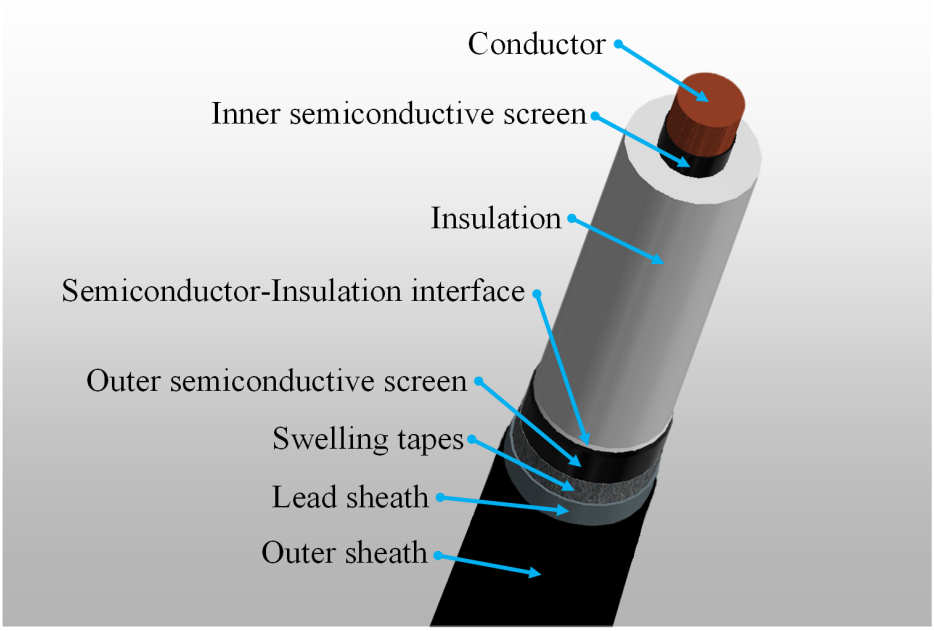

Figure 2.1: Description of the layers in a typical extruded submarine HVDC-cable.

Below follows a more thoroughly explanation of the different cable layers shown in Figure 2.1.

- The conductor is the part of the submarine cable that is carrying the current. The size and shape of the conductor is custom-made with consideration to the application, which means that the conductor can be manufactured in various configurations. The cross-section in Figure 2.1 shows a round-wired conductor and is made out of copper, further reading about commonly used conductor shapes can be found on pp.11 in [4].
- The inner semiconductive layer of an HVDC cable is implemented in order to even out the electric field created by the conductor and thereby prevent high stresses at single local points and protrusions, which can lead to electric breakdowns. The semiconductive screen is manufactured with the help of a semi-conductive material, i.e. carbon black [5], which is added to polyethylene. This material is then extruded around the circumference of the conductor.
- The insulation part of the cable is implemented in order to guarantee an efficient barrier from the high potential in the conductor to the grounded sheath. Since the cable insulation is exposed to very high potential differences, it is important to have an insulation with high chemo-physical purity and integrity (void free). This reduces stresses in single points of the insulation and thereby provide a longer lifetime expectancy [6]. The robustness of the insulation is also highly essential, together with the ability to withstand temperature and ageing. Plastics are commonly used insulation materials and for HVDC applications, where XLPE is most commonly used.
- The outer semiconductive screen has the same function as the inner one, with the difference of evening out the field towards the outside of the insulation. This again ensures no stress enhancement at local points or protrusions. It contributes together with the insulation and inner semiconductor to low leakage current that in the insulation, leading to low joule losses in the insulation system.
- The swelling tapes of a submarine HVDC cable are used to prevent water from longitudinally penetrating through the cable in case of external damages. It is often added close to the outer semi-conductive layer [6]. During an externally caused mechanical cable fault a part will be exposed to water, and could fail, but water penetration into a long section of the cable is prevented. Thereby, any repair made will not require scrapping of several kilometres of cable from the sea floor. The swelling tape should therefore ensure good water absorption and swelling if there is any water or humidity diffusion through the outer layers [7].
- The lead sheath is the part of the cable that creates the outer barrier against any water ingression. Since lead is a soft metal with relatively low melting temperature, manufacturing, transportation and installation of a metallic layer can be realised, and requires additional precautions to prevent any mechanical damages.
- The outer sheath of the cable is implemented in order to bring strength and protection to the lead-sheath that is placed underneath. The outer sheath is commonly manufactured from plastics, similar to the insulation layer.

Additional layers not depicted could include several armouring and protective layers, which are used to give strength to the cable and allow for deeper installation depths. During the installation of the submarine cable, the cable must bear its own weight down to the sea bottom, during which considerable tensile stresses are present and carried mostly by the armouring, and to some part by the conductor of the cable. Since the focus of this project is to analyse an extruded submarine HVDC-cable, a short description of the triple-extrusion-process for the cable depicted in Figure 2.1 is needed. In general, the extrusion-process consists of a perfect balance between heating, cooling and line speed, to control melting, chemical crosslinking and relaxation of the polymeric chains during the process [6]. In this triple-extrusion-process all three layers of the insulation system; the semi-conductive screens and the the insulation, are directly extruded over the conductor. This is done in order to avoid contamination and to ensure a smooth layer on the conductor surface, minimising enhanced field in certain points during utilisation. After the triple extrusion process, the insulation system is degassed when the cable is spooled onto a drum or a larger basket. This removes chemical crosslinking by-products from the insulation system, improving the chemical purity and ensuring low leakage current during operation.

2.1.1 Insulation

The insulation of an HVDC cable generally consists of mass-impregnated paper or cross-linked polyethylene (XLPE) [2]. In this master thesis the focus is on XLPE as the insulation material. To further increase the understanding of how cross-linked polyethylene behaves while being subjected to an electric field first a comprehensive literature study of the molecule structure of polyethylene is made in this section.

Polyethylene the most produced plastic in the world [8]. It consists of a high number of ethylene repeat units, which is a hydrocarbon (C_2H_4), forming a long chain of molecules usually called ”polymer”. The word polymer is a combination of the two Greek words ”poly” and ”meros”, meaning many and parts respectively. It is very intuitively that a polymer thus is a chain of many units, for example in the case of polyethylene poly denotes that there are many ethylene parts. The mechanical properties of the polymer is mostly dependent on two factors [9]:

1. The numbers of repeat units which is proportional to the length of the polymer chain in case of linear chain configurations. Another denotation for this is relative molecular mass. abbreviated RMM.
2. The shape of the polymer also has a significant impact on the mechanical properties.

The polyethylene molecule is formed by addition of ethylene monomers. The principle is to subject a reactor filled with ethylene monomers to high controlled temperature and pressure; initiating the necessary reactions for chain growth. An ethylene monomer and a polyethylene chain end including a free radical has the following chemical structure, respectively:

During chain growth the ethylene monomer will get attached to the polyethylene molecule end (at the black dot) and thus open its double bond. One of the carbon atoms of the ethylene monomer is thereby satisfied, the other one however still wants one more electron and will eventually find another ethylene monomer. It will get added to the polyethylene molecule in the same fashion and this is how the polymer chain grows.

Depending on the conditions during the polymerisation process the shape of the polymer chain will be different. Three of the most common shapes of polyethylene are; low density polyethylene (LDPE), high density polyethylene (HDPE) and cross-linked polyethylene (XLPE) [10]. The polymer conformations are illustrated in Figure 2.2. Differences between LDPE and HDPE, in short, is the occurrence of what is called "side-branches". These occur when the polymer molecule instead of adding an ethylene monomer to its chain end instead steals a hydrogen atom from a neighbouring already completed main chain (chain transfer) which means that the end is now terminated since the last carbon atom has its outer shell filled with electrons. However, since one hydrogen atom was stolen there is now an unfulfilled carbon atom of the neighbouring polymer chain and it will seek to attach an ethylene monomer. Therefore the polyethylene molecule will continue to grow but from another point. A longer side-branch has been formed. Another process, chain backbiting, occurs when the radical moves back a few positions along the same chain and chain growth continues from the new position, resulting in short branching.

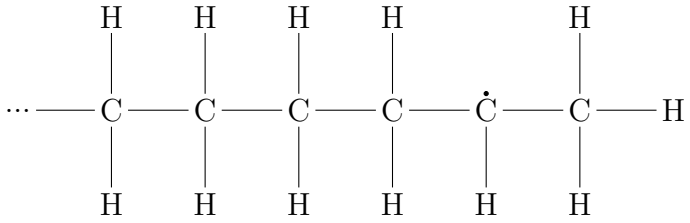

LDPE is characterised by approximately three side-branches per one hundred carbon atoms in the main-chain [9]. The fewer side-branches the tighter and more ordered these molecules can arrange themselves in crystalline (lamellar) structures, increasing its density. The low density of "low-density polyethylene" is therefore related to a higher amount of side-branches. HDPE on the other hand has about one side-branch per one hundred carbon atoms, and thus is easier to pack densely hence the name "high-density polyethylene". XLPE is different from the others since it is cross-linked which means that it is connected to a large network through different cross-links. By adding peroxide to, usually, HDPE or LDPE at lower temperature and then extruding the mixture, still below the decomposition temperature, and finally, vulcanizing it at temperature exceeding the decomposition temperature, it will become cross-linked. When the peroxide decomposes, it steals hydrogen atoms

from the chains, forming free radicals on them. When two radicals on different chains meet, a covalent bond is formed between the chains, creating the crosslink. It can be said that out of these three different shapes of the polymer chain XLPE is generally the one with the greatest mechanical properties in form of tensile and impact strength [9]. Another important difference between the three polymeric shapes is that XLPE is *thermoset* while LDPE and HDPE are *thermoplastic*. Thermoset means that a polymer is fixed in shape, meaning that even if it is heated beyond its melting temperature, it will keep the same form (except when it is heated to such degree that the covalent bonds of the carbon atoms breaks). Thermoplastic is the opposite of thermoset, if the polymer is heated beyond the melt temperature it will be moldable and able to change shape [11].

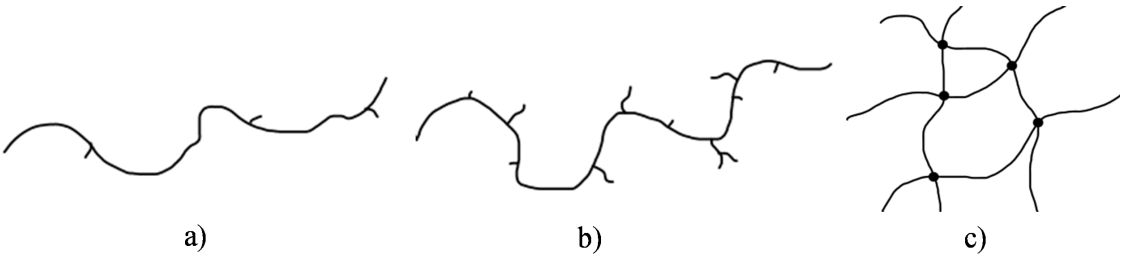

Figure 2.2: Shape of the polyethylene molecule depending on polymerisation process. a) HDPE, b) LDPE and c) XLPE

To further expand on the fact that HDPE packs more densely than LDPE another term can be introduced called *crystallinity*, which is the degree of how structured the molecules are inside a material. Polyethylene is crystalline to some degree at room temperature, and naturally HDPE is more crystalline than LDPE. Generally it can be said that irregular molecular structure inhibits crystallinity, as side branching prevent lamellear growth. A polymer is not fully crystalline but only semi-crystalline, which means that it is also *amorphous*. This is a combination of the Greek words "a" and "morphé" meaning without and shape respectively. The amorphous parts of the material that is non-crystalline is figuratively speaking "sandwiched" between crystal plate-like structure, usually referred to as *lamellae* [11]. The crystallisation of the material begins after the specimen is heated to its melting temperature, denoted by T_m, and then cooled to a lower temperature. When polyethylene is at T_m it will become amorphous, which means it will become transparent (it is non-transparent at room temperature), once it is cooled down to a certain temperature spherulites will start to form [9]. These spherulites starts growing from a nucleus and will expand in a radial direction as the time increases, as is depicted in Figure 2.3.

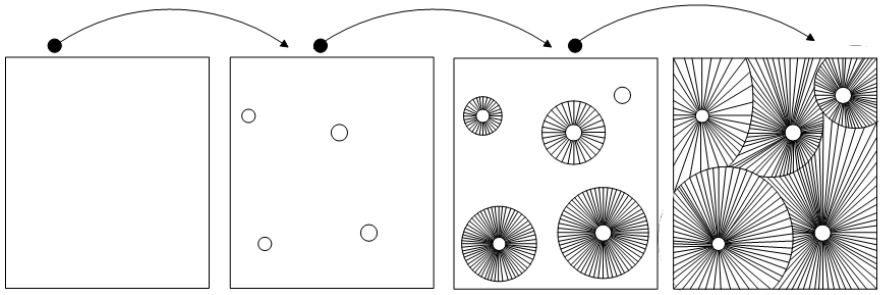

Figure 2.3: The growth of spherulites in a material. Straight lines indicate lamellae (not to scale).

When polyethylene was heated to above its melting temperature, the crystalline structure was removed, but when cooling from the melt the spherulites grow as more and more chains get attached to the crystal structure. The spherulites thereby grow, and this process continues until it makes contact with another spherulite or if the material itself has irregularities or some kind of impurity which inhibits the crystallisation.

Except the melting temperature, T_m, there is another temperature that is important when discussing polyethylene and that is the glass transition temperature, T_g. It is the temperature when a polymer goes from glass to either rubber or liquid. The glassy state of a polymer is when the polymer backbone is immobile, once the temperature passes above T_g the polymer enters the liquid/rubber state and the molecules are again mobile. For XLPE the glass transition temperature is far below room temperature. Therefore, chain mobility is allowed in the material during all operation conditions.

The mechanical properties of a crystalline polymer can further be improved by making it an *oriented structure* [9]. Consider several polyethylene molecules randomly oriented, figuratively the chains can be compared to spaghetti. If the temperature is above the glass transition temperature, T_g and the material is extended followed by a quench, cooling the material rapidly, it will get an oriented structure as the polymer chains no longer are randomly oriented. This process can be observed in Figure 2.4. Whereas this process is highly utilized in fibre-forming, for polyethyle the glass transition temperatures is far below room temperature. Locking in the polymer orientation is thus not possible. However, during the cable extrusion process, the material passes through a narrow slit in the extrusion head. When passing the extrusion head, the polymer can therefore end up with different morphology (crystalline shape) than compared to a polymer prepared in a press-molding technique. There are several properties that affect the electrical conductivity of an insulating polymer, one of these is morphology. With increasing orientation of the polymeric chains the conductivity generally decreases for semi-crystalline polymers such as polyethylene [12].

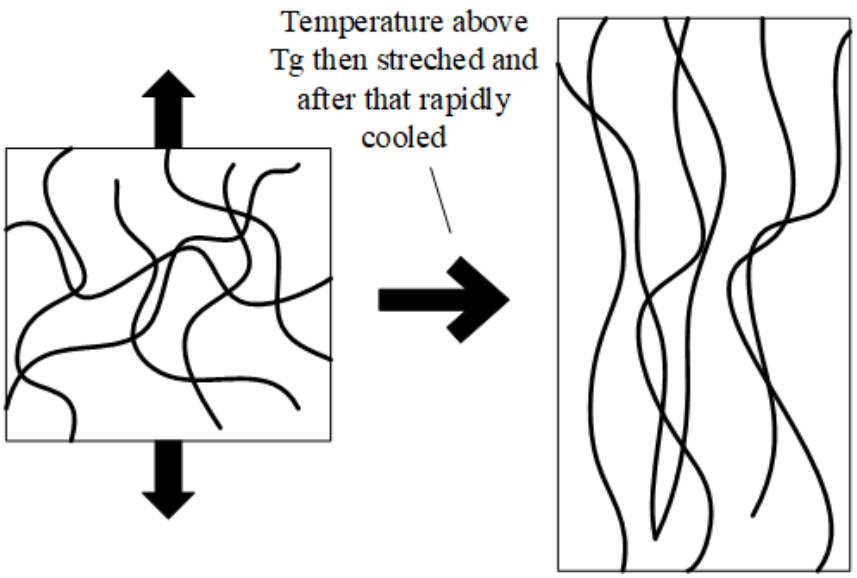

Figure 2.4: The process of converting a semi-crystalline polymer from more being randomly oriented to more non-randomly oriented, during mechanical stress or cable extrusion.

2.1.2 Semi-conductor

In Figure 2.1 it can be seen that there are two semi-conductive layers in an HVDC extruded cable; an inner and an outer. A typical method of making these semi-conductive layers is to fill polymers with for example *carbon black* which is semi-conductive. The polymer semicon in this specific project is also polyethylene which later is cross-linked by adding peroxide, similarly to the insulation [13]. In HVDC cable applications acetylene black is used due to its chemical cleanliness and low roughness of the semi-conductive mixture [14], and is produced by thermally decomposing acetylene gas. Having a semi-conductive layer is important in order to prevent electrical degradation and an eventual breakdown, since it inhibits the accumulation of space charges in the insulation as it reduces local field enhancement [14].

There exists different types of carbon black, one was mentioned in the previous paragraph (acetylene black) and another common variation is *furnace black*. What separates these two is the manufacturing process and it in turn yields different material properties [15]. It was shown in a study performed by U.H. Nilsson and J-O. Boström that acetylene black is more suitable for cable applications due to its ability to inhibit accumulation of space charges in the insulation [14]. Another aspect that is important when regarding insulators with added conductive fillers, such as carbon black, is that it requires a certain concentration of the filler material to transform the insulator to a semi-conductor. However if the concentration is further increased the conductive abilities of the compound will eventually reach a steady-state value and will not increase more [13]. This effect is referred to as percolation.

2.2 Electric conductivity of insulating polymers

Conductivity is the inverse of electrical resistivity and a measure of how well a material can conduct an electric current. The expression for electrical conductivity is:

$$\sigma = \frac{1}{\rho} = \frac{1}{R\frac{A}{L}} = \frac{J}{E} \tag{2.1}$$

and has the unit of $[(\Omega m)^{-1}]$. To give a brief introduction to the concept of electric current, it is the transportation of charge and has the unit Coulomb per second (often referred to as Ampères). The two main transport mechanisms are; drift and diffusion [16]. Drift of charge carriers occur when an electric field is applied which causes an electrostatic force that moves the charge carriers. Diffusion causes the charge carriers to move due to the occurrence of a concentration gradient and random movement. The conductivity can be expressed as according to [16]:

$$\sigma = e \times (n\mu_n + p\mu_p)\ [(\Omega m)^{-1}] \tag{2.2}$$

$$\mu = \frac{v_d}{E}\ [cm^2/Vs], \tag{2.3}$$

where e denotes the elementary charge, n and p the concentration of electrons and holes, μ_n and μ_p the mobility of electrons and holes. v_d is the drift velocity of the charge carriers. In this section relevant theory will be presented to understand how the concept of conductivity applies to polymers.

2.2.1 Energy band theory and its application to polymers

According to the Pauli exclusion principle, two electrons cannot have exactly the same energy if they are occupying the same room [11]. In other words this can be explained as each energy state can only house one electron. However, when atoms are very close to each other the electron orbitals can somewhat overlap. The energy of the electrons cannot be the same, which means that there will be a slight difference in the energy. When a lot of atoms are gathered together in this manner they collectively form a molecule or crystalline solid, this will result in a lot of overlapping electron orbitals and multitude of different energy levels. The difference between the lowest energy level and the highest energy level of the electrons become what is called an *energy band*, in Figure 2.5 an illustration of the energy band concept is depicted. Between two energy bands there exists a gap where there are no states (or bands) housing electrons, this space is called a *band gap* [16]. The bottom of the band gap is named the *valence band* and the top of it the *conduction band*.

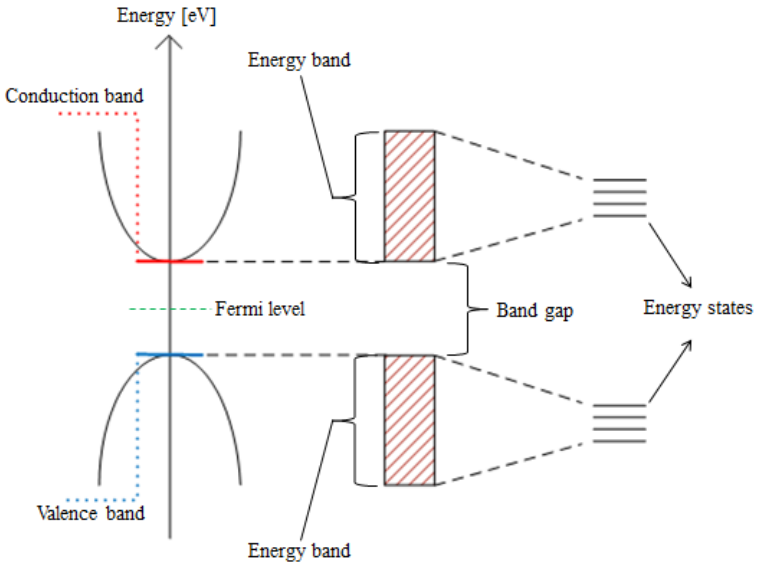

Figure 2.5: A simple illustration of how energy bands and band gaps are formed.

Formally, it can be said that the band gap exists between the bottom of the conduction band and the top of the valence band. In the band gap an electron cannot acquire any energy, which in other word means that there does not exists any states that can house an electron [16]. Now that the principle of band theory has been explained some relevant terms will be presented.

- Vacuum level - this is used as a reference value in order to compare materials. It is the energy of a stationary electron in vacuum.
- Ionization energy - this energy is defined as the energy level of the electron subtracted by the vacuum level. In other words it is the minimum energy required to excite an electron such that it leaves the atom, thus resulting in a positive ion and a free electron.
- Fermi level, E_F - the definition of Fermi level is such that if there is an electron state at the Fermi level, then the probability of that state housing an electron is 50% according to the Fermi-Dirac distribution function [16].
- Work function, Φ - is defined as the energy needed to move an electron from the Fermi level out of the atom, in other words to the vacuum level.
- Electron affinity, χ - can be described as the energy released as an electron becomes accepted by an atom, thus forming a negative ion. Another way of describing it is as the energy needed to remove an electron from the lowest point of the conduction band.

If the energy is high enough an electron can be excited from the valence band to the conduction band, thus enabling it for conduction since an electron in the conduction band has a higher energy than the Fermi level. This will leave behind a missing electron, a hole in the valence band, which essentially is a positive charge carrier. According to equation (2.2) the conductivity is depending on the mobility of holes and electrons as well as the amount of them respectively. Mobility can be expressed as equation (2.3), but it can also be expressed as

$$\mu = \frac{e\tau}{m^*} \; [cm^2/Vs], \tag{2.4}$$

where e is the elementary charge, τ is the mean time between two consecutive collisions of an electron and the crystal lattice and m^* is the effective mass (which is different for holes and electrons). This indicates that the mobility is strongly dependent on temperature, in turn this means that the conductivity itself has a significant temperature dependency [11].

The band gap itself can be used to give a quantitative description if a material is conductor, semi-conductor or insulator. According to [11] these are:

- Conductor - a material with a band gap below ~ 0.2 [eV], for example an energy band could only be half-filled, such that no energy gap seemingly exists.
- Semi-conductor - a material with a band gap between 0.2 - 2.0 [eV].
- Insulator - a material with a band gap above ~ 2.0 [eV].

2.2.2 Electronic conduction within the insulation

As been stated in previous section, for insulators and semiconductors, hole and electron pairs need excitation in order to be created, requiring the addition of sufficient energy in order to be transported through the energy band. In this section there will be a more thoroughly explanation about electronic conduction in the regions where the thermal energy is not adequate for the excitation through the energy band. Worth mentioning for this section is that the extrusion-process results in residues, which will leave impurities in the material and lead to energy states, traps, between different molecules and at defects of the molecular-chain [17]. Such residues, can themselves also transport upon ionisation, which we will not consider here. Additional traps can originate from other chemical defects in the material, as well as physical disorder [11]. These localised states will trap the electrons and holes until sufficient energy is gained, which means that trapped charges are not accessible for conduction. In Figure 2.6a the traps within the energy band of the insulation are visualised.

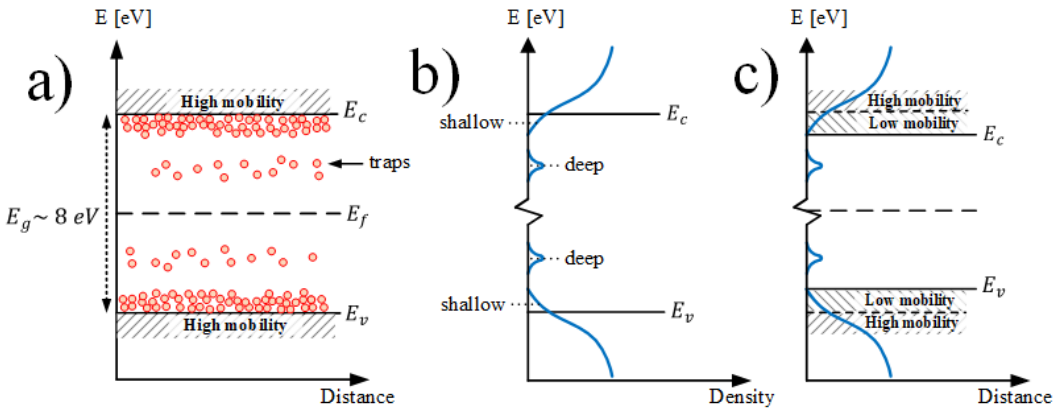

Figure 2.6: The extended model of the energy band (E_g) for polyethylene. (a) A more realistic representation of the energy band with the impact of states and traps. (b) Description of the new energy states in turns of trap-density. (c) The modelled energy states included in the energy band.

As can be seen from Figure 2.6a the traps are placed at different energetic depths and, additionally, are present in different densities. This means that the required energy for carriers to remain free and conduct in the material depends on the various potential barriers of the traps. Since the potential barriers of the traps are of sufficient size, it can be stated that the transportation of carriers cannot be explained by the thermally excitation to the conduction band due to unreasonably high temperature levels. A phenomena that explains the electron- and hole-transportation, at reasonable temperature levels, is thermally activated hopping. This mechanism states that the electrons and holes jump between the different traps, without reaching the conduction band, due to the energy gained from the thermal fluctuations within the lattice. As this transportation mode additionally involves quantum mechanical tunnelling, spacing in between the different trap sites is of importance. This will in turn result in a conduction of carriers through the material, where the conduction rate is mainly dependent on the distance and depth between the adjacent traps and not the characteristics of the conduction band.

The different states/traps causes the charge transport to vary throughout the material and can be explained with the extended model of the band-gap, which is a more adequate presentation of the energy band with the impact of the traps and is visualised in Figure 2.6b and 2.6c. In the figures new energy levels that account for the different states of the charge carriers are introduced. The traps located close to the edge of the conduction band are modelled as ”shallow-traps”. In this region the charges will jump between the different traps, hopping, and thereby assist the charge transport. This is why the conduction band is located at a lower level in Figure 2.6c compared to the conduction band in Figure 2.6a. The mobility of the charge carriers is low within this region, since the carriers will be trapped in the states for some time before reaching other states. This implies that the conduction through the insulation highly depends on the ”depth” of the traps, the trap concentration and on the detrapping mechanism. The traps located at deeper levels are modelled as the ”deep-traps”. These traps will also affect charge transport, as here charge carriers are trapped for longer times. Additionally, no hopping occurs between the deep traps as their density is significantly lower. The deep traps will thus allow the material to store charge for longer time and further reduce the conductivity of the material.

2.2.3 Macroscopic conductivity expression

While the previous section has described conduction from a charge carrier standpoint, we will here present a macroscopic conductivity expression and reflect on the origin of its dependencies. The klein's conductivity expression for the bulk conductivity, with electric field and temperature dependency, is:

$$\sigma = \sigma_0 e^{(\beta T)} e^{(\alpha E)}, \tag{2.5}$$

where σ_0 is the conductivity without temperature and field dependency, T is the temperature expressed in its measured unit, α $[1/^\circ C]$ and β $[(kV/mm)^{-1}]$ are constants and E is the energy level in [eV]. From the equation, during uniform field, it can be observed that the conductivity is strictly dependent on the temperature. The temperature and field dependency originates from the expression for the hopping conduction, found on pp.223 in [11]. From the expression it can be realised that the conduction, due to the hopping mechanism in the shallow traps, have an exponential temperature and field dependency. Additionally, trapping and detrapping to deep traps also feature strong field and temperature dependencies. It is evident that the macroscopic conductivity equation thus is an average over all the conduction processes occurring within the material.

2.2.4 Reduction of impurity content

As been stated in section 2.1.2, peroxide is used as catalyst during the vulcanization process to form the specific chemical structure that is demanded of the cross-linked polyethylene. Utilising peroxide as catalyst generates residues within the specimen and form cumylalcohol, methane, acetophenone and alfa-methylstyrene [11]. These unwanted byproducts impact the conductivity by changing the impurity rate and in turn the trap concentration in the energy gap. This implies that the conductivity increases with an increment of byproducts from the catalyst. Additionally, such residues can, upon ionization, transport in the material and again increase the conductivity. In order to reduce the impurity content and minimise the impact on the conductivity, the specimen can be heated to a temperature, below T_m, which allows for faster outgassing these residues. This process is called degassing and is performed after the extrusion procedure of the HVDC-cable. During subsequent electrical screening tests the outgassing occurring during the extrusion process alone is thus not enough to minimise the impurity content and a this second degassing process is performed. During the secondary degassing process the byproducts will be further evaporated but this will also lead to an increase in crystallinity of the specimen. The reason for this is that the small crystals that were created during material cool-down after cross-linking will melt and combine with other crystals. Therefore, larger crystals will be formed during the reheating and in turn increase the crystallinity. This phenomena is called thermal annealing and is a way to further explain the grow rate of larger crystals close to the melting temperature over a certain period of time. This implies that specimens follow a different degassing process might result in a different morphological structure and residue content, in turn impacting the conductivity.

2.2.5 Charge injection on metal-polymer interfaces

In order to measure the leakage current in both peeled and moulded samples, a test cell (explained and depicted in section 3.2.2) with a high-voltage electrode connected to the semi-conductive part of the specimen. The interface between the electrode and the semiconductor consists of different materials, where the electrode is made of metal and the semi-conductive screen is produced from carbon black. These parametric differences, chemical impurities and roughness of the surface will lead to an interface where the Fermi levels do not align [18]. This phenomenon can be observed in Figure 2.7a. The situation can be simplified since the electric field will be approaching zero within the semiconductor. Therefore, it is not the metal-semiconductor interface that controls the charge injection rate within the samples and within HV cables, but rather the semiconductor-insulation interface. This simplification is indicated in 2.7b.

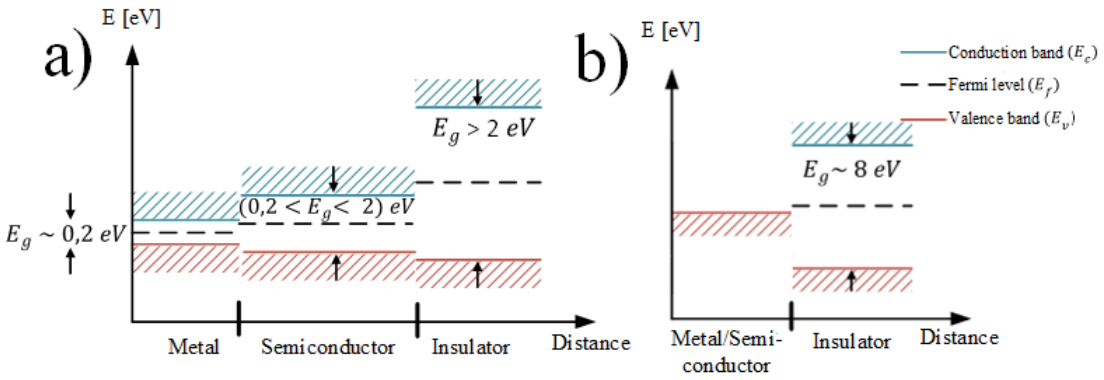

Figure 2.7: (a) The level of the energy band for the different interfaces in the test cell.(b) The energy band model implemented on the semicon-insulation interface. The ground electrode is not shown.

The simple energy band presented in Figure 2.7b assumes a sharp and steep transition between the semiconductor-insulation interfaces. In order to model this scenario with impact of external parameters, the Schottky barrier model can be used [11]. Traditionally, this model states that there will be a depletion layer within an semiconductor due to a charge transfer from the semiconductor to the metal until the Fermi levels align. However, since no excess carriers exist within an insulation this band bending process is not applicable for insulators [11].

As stated, the interface between the semi-conductive part and the insulation will not experience any exchange of carriers, since there are no major charge carriers within the insulation [11]. This results in a sharp transition between the semiconductor and the insulation. During the impact of electric field in the insulation the energy band will bend in accordance to the direction and level of the field, which is illustrated in Figure 2.8b. Electrons that have entered the insulation will due to the law of the

image charge effect [11], create an electric field that impacts the barrier presented in Figure 2.8a [19]. The field from the electrons in the insulation will bend the band even further and the barrier can be remodelled as is shown in Figure 2.8b.

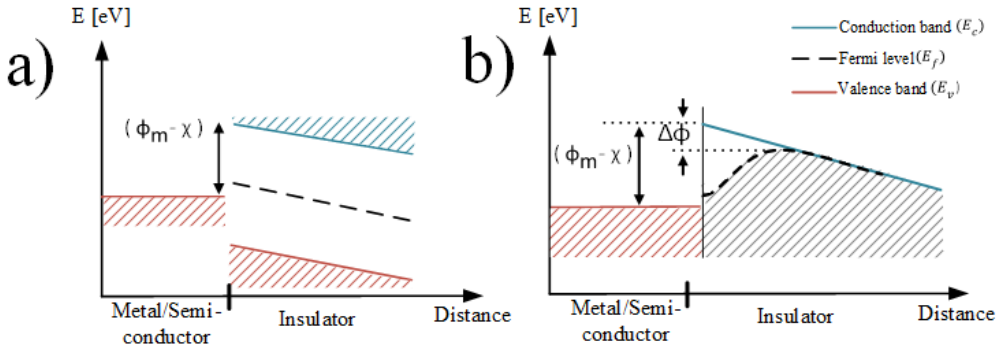

Figure 2.8: (a) The energy band of the metal-insulator interface during the impact of electric field. (b) The extended model for the field lowering effect of the Schottky barrier on the metal-insulation interface.

The barrier height of the energy band presented in Figure 2.8a and 2.8b is equal to the difference between the work function of the metal Φ_m and the electron affinity χ. Typical values for the work function of metal is approximately 4-6 eV and around 3-5 eV for the electron affinity of semiconductors. The electron affinity for the insulation, XLPE, is approximately -1 eV [2]. The negative notation of the electron affinity indicates that there will be an increment of the total barrier height. The field lowering effect presented in Figure 2.8b will experience a lower barrier height and the difference in height is represented as $\Delta\Phi$, which in turn impacts the charge injection rate from the metal. In equation (2.6), derived on pp.218-222 in [11], the charge injection for the Schottky model is presented and assumes the following expression:

$$J = \frac{4\pi e m k_b^2 (1-R) T^2}{h^3} \exp\left(\frac{-\Phi}{k_b T}\right) \exp\left(\frac{e}{2k_b T}\sqrt{\left(\frac{eE}{\pi\epsilon\epsilon_0}\right)}\right). \tag{2.6}$$

The equation consist of many different physical parameters, material constants and variables that are further explained on pp.222 in [11]. From the equation it can be observed that the charge injection is highly dependent on the temperature (T), the electric field (E) and on the difference in barrier height (Φ). This implies that variance within temperature and field is of high importance when analysing the current density throughout different interfaces of an HVDC-cable. As equation (2.6) states temperature and electric field heavily affect the injection current density, this will in turn affect the conductivity since there is a relationship between the two. The injection process is thus another phenomenon included within the macroscopic klein's conductivity expression described by equation (2.5).

Another factor that is of great importance when performing conductivity measurements is the contact pressure, in other words the pressure applied to the sample by the electrode. It was shown in a study performed by X. Liu and D. W. Schubert that a higher contact pressure will result in a higher conductivity [20]. In the case for the semiconductor, e.g. carbon black, the conductivity is highly dependent on the concentration of conductive fillers as mentioned in section 2.1.2. If the pressure on the semiconductor is high then there will be internal stresses in the material which causes the contact resistance between the conductive fillers to decrease which in turn increases the conductivity of the semiconductor [21]. However, this effect is not necessarily what affected our results, as the field within the semiconductor was low. In our samples, the opposite electrode was a physical metal-insulation interface with an interstitial layer of dielectric grease. When contact pressure was increased, this interface was better mated and less noise was noted during the measurements.

2.2.5.1 Surface roughness

In the previous section the field lowering effect of the Schottky barrier is presented and used to explain the charge injection for the semiconductor-insulation interface. The internal roughness of the semiconductor-insulation interface, might impact the charge injection. In an article from the Department of Engineering Physics at Ankara University it is concluded that the surface roughness of semiconducting thin films highly impacts the electrical conductivity [22]. This result is of significant importance when comparing a peeled and press-molded sample, since the variation of the internal roughness are unknown. The roughness also determines how well the sample is in contact with the ground electrode. High surface roughness on the sample will lead to peaks and valleys across the contact surface, which in turn results in irregularities. These irregularities will cause an unevenly distributed field and the charge injection will vary across the sample.
When discussing surface roughness there are an abundance of parameters that have different significance for different applications and surfaces. The parameters studied in this master thesis are; S_a, S_q and S_{dq}. Arithmetic mean height, S_a is a measure of how much each point of a 3D surface deviates from its arithmetical mean [23]. S_a is often used to determine the roughness of a surface. The mathematical expression is as follows in equation (2.7) [23].

$$S_a = \frac{1}{A} \iint |Z(x,y)| dxdy \tag{2.7}$$

S_q denotes the root mean square height, and is the standard deviation of heights. It is determined with equation (2.8) [24].

$$S_q = \sqrt{\frac{1}{A} \iint \Big(Z(x,y)\Big)^2 dxdy} \tag{2.8}$$

Even though that S_a and S_q are commonly used surface roughness parameters they can be deceptive, since they are absolute values there is no indication of conformation of the surface in regards of peaks or valleys. This can lead to that two completely different surfaces can get the same value of S_a [25]. For this reason it is good to

consider a roughness parameter with a gradient, for example S_{dq}. It is the root mean square gradient and takes into consideration both the height texture and the spacing [26]. For example, a surface with smoother peaks or valleys and larger spacing between them would probably generate a lower S_{dq} than that of a surface with less spacing and steeper peaks or valleys, however the arithmetic mean height could be similar for both surfaces. The S_{dq} is expressed with equation (2.9) [26].

$$S_{dq} = \sqrt{\frac{1}{A}\int_0^{\mathcal{L}_x}\int_0^{\mathcal{L}_y}\left\{\left(\frac{\partial Z(x,y)}{\partial x}\right)^2 + \left(\frac{\partial Z(x,y)}{\partial y}\right)^2\right\}dxdy} \tag{2.9}$$

3
Methods

The aim of this project is to conduct measurements with reliable results and to ensure a solid test setup that works for different samples. Therefore, the method of this thesis has been the main part of the work. In this section the necessary steps for the construction of the test cell will be explained, together with equipment used and relevant programming for data communication.

3.1 Test samples

The electrical tests performed during this projected consisted of the comparison of the leakage current within peeled and press-molded samples. The following section presents relevant information about the manufacturing process for the different samples.

3.1.1 Cable peelings

The cable used for peeling manufacturing, provided from Nexans Norway, was a short piece of full-scale extruded HVDC-cable. This Cable had been priory electrically screened for defects and degassed. The peeling process started with the stripping of the cable until the outer semi-conductive screen was reached. This included manual removal of the outer sheath, lead sheath and swelling tapes. This was followed by a cleaning procedure with the aim of removing leftovers from the stripping. After the cleaning, the cable was placed in a sterile environment and a specially designed cutting-tool was used to make the peels. The cutting was done in the circumferential direction, following the surface. Since the aim of the report is to analyse the semiconductor-insulation interface, the surface of the outer semiconductive screen had to be removed until it could be guaranteed that the next extracted sample consisted of both semiconductor and insulation. The cutting tool was manually operated, which made it hard to calibrate and also lead to uncertainties of the sample-thickness. The extrusion process for an HVDC-cable is done automatically and in large quantities, which can results in slight deviation in the cable roundness. This variation resulted in different thicknesses along the lengthwise orientation of the extracted cable peeling. In order to increase the preciseness and reduce these uncertainties, a microscope was used to determine the thickness. Assessment of the thickness was done when all the electrical tests were completed, in order to prevent the risk of damaging the surface of the samples.

Before performing the electrical testing, the peeled samples went through an additional degassing process. This process was done by heating the samples to a temperature where residues are eliminated at a much faster rate, as mentioned in section 2.2.4. Since the thicknesses of the peeled samples were unknown during the degassing, the time for this process was adapted to thicker samples. This ensured the removal of most of the impurities, minimizing their impact on the conductivity. This time was chosen to be 24 hours. Whenever the peeled samples were not used, they were stored in an incubator with the purpose of dehumidification and thereby reducing the impact of external moisture.

3.1.2 Press-molded plates

In order to be able to measure how the orientation of the polymeric chains within the semiconductor-insulation interface impacts the conductivity, press-molded samples were manufactured. The press-molded samples were created to have a reference interface where the polymeric chains have more random orientation, compared to the peeled samples from the extrusion process. The samples were created in the material lab at Nexans Norway and the procedure is well known within the industry. In this process the semiconductor and insulation were fabricated separately and then pressed together, likely resulting in a higher degree in random morphological structure within the samples. Crystalline structure will still exist in these samples, but the additional molecular orientation from the extrusion process was not introduced in this manufacturing method. When pressing the plates a film is needed so that the samples become even do not stick to any of the parts used in the process. PET (polyethylene terephthalate) is commonly used, however there have been studies confirming that it affects the conductivity of the polyethylene press-molded samples [27]. In this master thesis kapton was used as press film instead of PET, as it has no documented effects on conductivity. This will be investigated by performing an electrical test with temperature cycling on a pure polyethylene press-molded sample. If similar results are acquired as the test performed by H. Ghorbani, et. al., then new press-molded plates need to be made with a different press film.

The press-molded process started by making separate plates, one for the insulation and one for the semiconductor. This was done by heating the material, under the impact of a force around 25 kN for 10 minutes, to a temperature just above T_m. The reason for not exceeding T_m more is that this will initiate the peroxide decomposition initiating the crosslinking reaction. When a temperature of 120 degrees was reached the sample was cooled down to room temperature during the impact of a force around 250 kN. During the final step of the manufacturing the separate plates were joined and again heated far beyond T_m, 170 degrees, initiating the peroxide decomposition, crosslinking the material and also bonding the interface of the two samples. The final pressing was done with a force of 25 kN for about 5 minutes and then increased to 250 kN for 20 minutes. The press-molded plate was then cooled down, during the impact of the same force, to room temperature finalizing the process. The process for forming the separate plates is visualised in Figure 3.1a and joining and crosslinking of the press-molded plate is presented in Figure 3.1b. The insulation thickness within the press-molded plates could be obtained with a simple measuring

tool and was done by measuring the thickness of the plate in advance to joining the semiconductor to the insulation. The degassing time for the press-molded plates was chosen to 48 hours, which is longer compared to the peeled samples. The reason for this is that the peeled samples had a priory low residue content, owing to the degassing process during the manufacturing of the cable. The degassing time for the press-molded samples was again selected in order to keep the impurity content as low as possible. Whenever the press-molded samples were not in use, they were stored in the same incubator as the peeled samples.

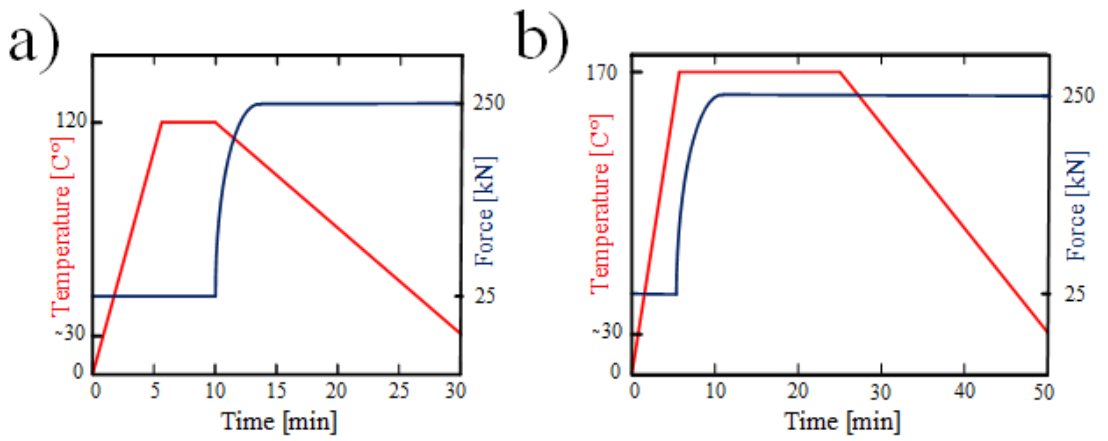

Figure 3.1: The process for the press-molded "sandwich". (a) The procedure for the insulation and semiconductor plates. (b) The construction of the finalised plate, where the separate plates are pressed together and crosslinked.

3.1.3 Optical profilometry

In order to assess the surface roughness of the press-molded and peeled samples, optical profilometry analysis was performed. The surface was scanned with a Wyko RST plus interferometer, utilising white light interferometry. This scanned a light pattern over the surface at different focal depths, generating spatially dependent reflections on the surface. These readings were saved as X,Y,Z coordinates, and could be further analysed with the aid of different software. The post processing of the data was done in MATLAB™ and enabled the possibility to plot the scanned surface and calculate the S_a, S_q and S_{dq} parameters. These parameters are used to assess significant variations on the surface, were S_a is mainly used for machined surfaces and S_q together with S_{dq} to analyse optical surfaces.

3.2 Test set-up

For this project three different test-cells have been benchmarked to see which provides best results. In section 3.2.2 the two test-cells designed by Espen Doedens, one with a secondary guard ring and one without, are presented and explained. Henceforth the test-cell without guard ring and with guard ring will be abbreviated to TC1 and TC1-G respectively. Furthermore, the test-cell designed by Xiangdong Xu is described in section 3.2.3, and will further be abbreviated to TC2.

3.2.1 Test-set up TC1, TC1-G, TC2

The test-set up is presented in this section, and the main parts can be observed in Figure 3.2 and are further noted in following list:

- Test-cell
- High voltage source Glassman EH-series, 50 kV
- Keithley 6517B Picoammeter
- PC for data acquisition and treatment

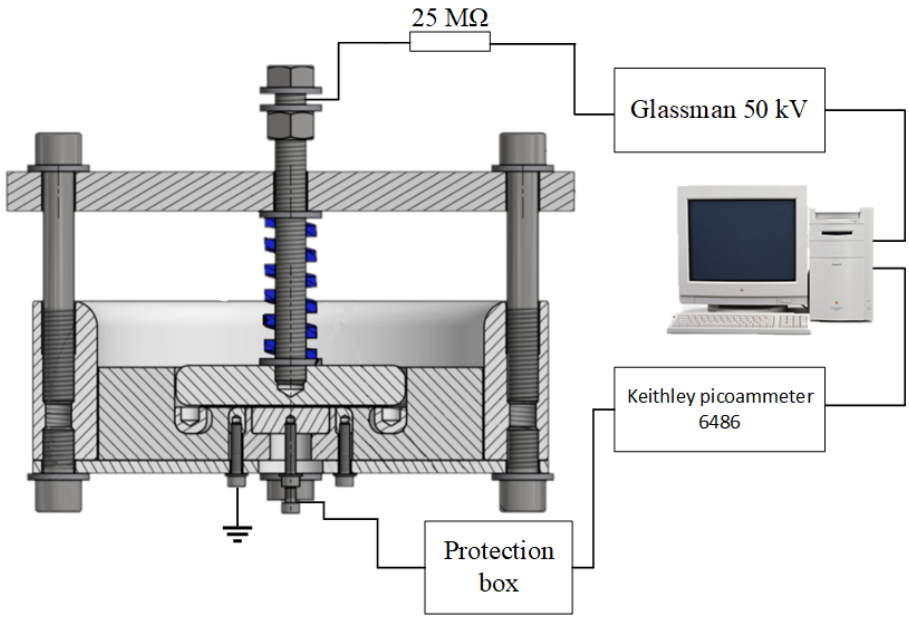

Figure 3.2: Simple schematic of how the TC1-G is connected and what instruments are used.

The set-up is exactly the same for each test-cell with the only difference being which test-cell is used, which in Figure 3.2 is TC1-G.

3.2.2 Test-cell TC1 and TC1-G

This test-cell was designed by the supervisor, Espen Doedens, for this master thesis and was manufactured by the Norwegian company Sørlie. Two test-cells were made, one with a secondary guard ring and one without. The one depicted in Figure 3.3 is the one with a secondary guard ring, the only difference between TC1 and TC1-G is as mentioned the occurrence of this secondary guard ring or not. The test-cell contains following key points, as can be seen in Figure 3.3.

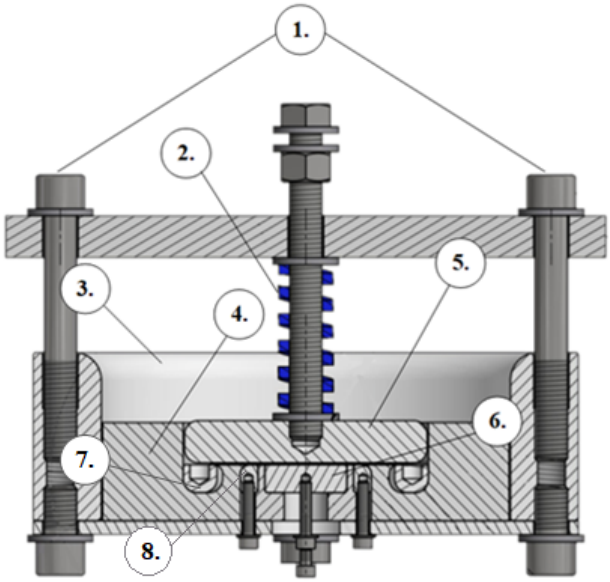

Figure 3.3: The TC1-G and its different key components.

(1) Hexagon socket head cap screw, M12, stainless steel.
(2) Bordignon spring ISO series 150mm, shortened to 50 mm.
(3) Aluminium body of the test-cell.
(4) Insulating block, HDPE insulation.
(5) High voltage electrode.
(6) Measuring electrode.
(7) Secondary guard ring.
(8) Inner guard ring.

The principle of the test cell is that high voltage is applied to the high voltage electrode via the Glassman power supply (further explained in section 3.2.6) which is connected to the top of the bolt with the bordignon spring. The sample, either cable peeling or press-molded plate, is placed between (5) and (6) in the test-cell with the semi-conductor side facing the high voltage electrode and the insulation side facing the measuring electrode and guard ring. The connection between the measuring electrode and the Keithley 6517B is made by a modified coaxial cable, where the copper core is connected straight to the measuring electrode and the shield is connected to the test-cell body, which in turn is grounded. By turning (1) the pressure on the sample increases and can be further studied in 3.2.5.

3.2.3 Test-cell TC2

The following list presents the necessary parts of TC2.

(1) Outer shell, brass, which is grounded.
(2) Current measuring electrode, brass.
(3) Conductive rubber.
(4) High voltage electrode, brass.

The principle of this test-cell is that high voltage is applied to (4), between (2) and (4) a sample is placed. The leakage current is then measured in the same fashion as for TC1 and TC1-G, by a picoammeter connected to the measuring electrode via a modified coaxial cable.

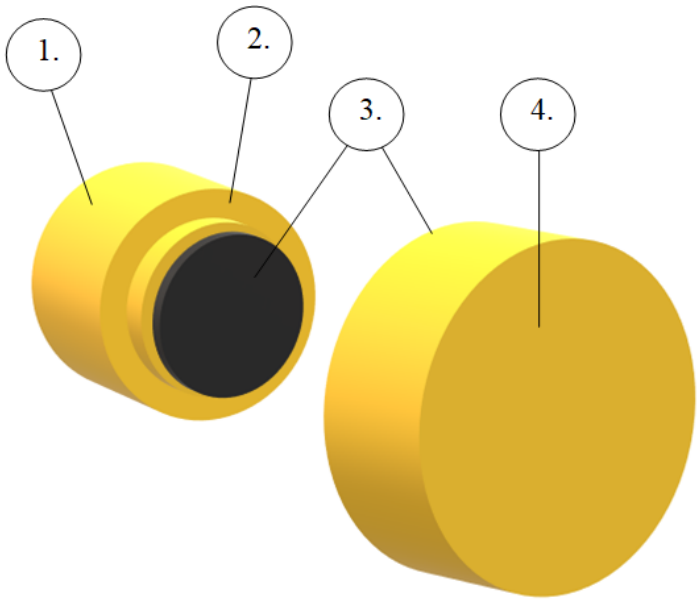

Figure 3.4: Illustration of the necessary parts of TC2.

3.2.4 Safety measures for the test set-ups

To ensure that the high voltage tests were done in a safe environment additional safety measures for the test cell were required. The parts of the cell that were exposed to high voltage, voltage above 1,5 kV DC, were placed within a grounded cage or within a heating chamber. This in turn guaranteed that faults within the cell would be conducted through the chamber and not to the surroundings. To prevent ambient discharges from the connections to the power supply these connections were placed within high voltage toroids, which evens out the field and reduces enhanced field points.

In the occurrence of a breakdown the test cell would experience full short circuit current, which is the maximum current that could be supplied from the power source. To prevent the cell from being damaged, a current limiting resistor was placed in series with the connections from the power supply and was chosen to 25MΩ. During a breakdown in the test cell the maximum current that the resistor could experience

was 10μA, which was the set limit that was chosen of the power supply. This would lead to a voltage drop of around 250 V in the resistor. The power developed in the resistor during a breakdown would then be 500 μW and was considered harmless. In order to keep the Keithley out of harms way during a breakdown a protection box was used. The protection box was connected from the low voltage side of the test cell to the picoammeter, as can be observed in Figure 3.2. Further, a stop function was implemented in LabView, such that if the current exceeds a value set by the user it will stop the program and set the test voltage to 0 V.

3.2.5 Pressure calibration

Since the aim of this project was to analyse and compare different readings from the measurements, elimination of uncertainties was of high priority throughout the process. The pressure subjected to the sample during the measurements had to be accounted for and were controlled by the cap screws and the spring in the test cell, (1) and (2) respectively in Figure 3.3. The calibration of these springs was done manually with the help of a scale. In this procedure the scale worked as a substitute for the sample and each rotation of the springs could be measured in kilogram. The scale had a maximum limit of 5 kg, which only made it possible to measure the pressure up to that limit. These values were then easily converted to get the pressure in bar per rotations and can be observed in Figure 3.5.

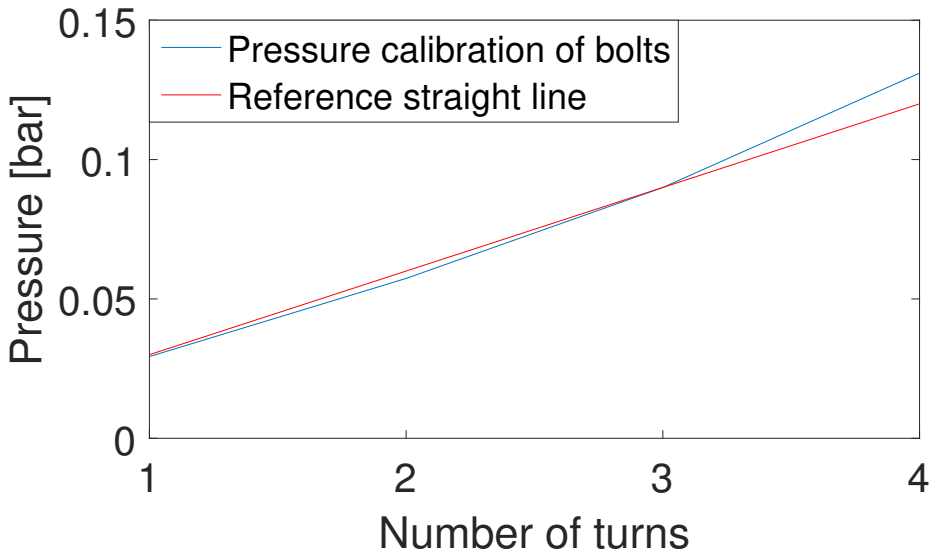

Figure 3.5: The pressure experienced by the sample within the test cell per rotations of the bolts.

With the pressure from the rotations of the spring, that is shown in Figure 3.5. The measurements could be done during equal pressure and led to a more consistent testing procedure. Interface pressure was hereby controlled during the experiments.

3.2.6 High voltage circuit

The Glassman power supply generates a DC voltage of 0 kV to 50 kV and is controlled by an input DC voltage of 0 – 10 V, meaning that for example 1 V input voltage will generate 5 kV output voltage. An overview of how the power supply is controlled is displayed in Figure 3.6.

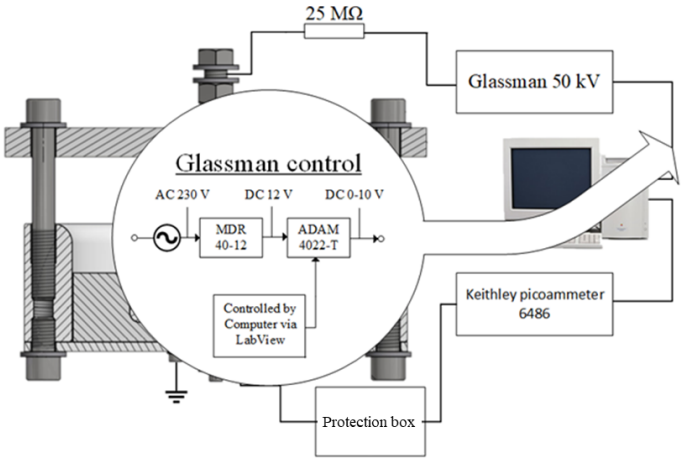

Figure 3.6: In-detail schematic of how the Glassman high voltage power supply is controlled.

First AC 230 V is taken from an ordinary power outlet and is then converted to 12 V DC by the MDR 40-12. This DC voltage is in turn the input voltage for the ADAM-4022T device. The ADAM-4022T essentially takes an input voltage and outputs DC 0 – 10 V depending on what command it is given by the computer, and has an accuracy of ± 0.15%. The computer communicates with the ADAM-4022T via RS485-USB converter and is controlled via a LabView program such that it can output any voltage between 0 – 10 V, which in turn makes the Glassman output 0 – 50 kV. The ADAM-4022T can be used for several different applications but in this case, as it is stated, it is used to output DC 0 – 10 V. In Figure 3.7 the different ports of the ADAM-4022T can be observed.

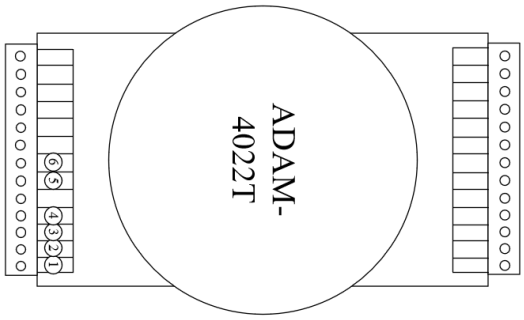

Figure 3.7: Overview of the ADAM-4022T device and its different ports.

The ports of interest to make the device operate as a power supply are marked in Figure 3.7 and are:

1. Ground
2. Vs+
3. DATA-
4. DATA+
5. AO 0 COM
6. AO 0

The MDR 40-12 is connected to Vs+ and Ground, and the RS485-USB converter is connected to Ground, DATA- and DATA+. The output is generated at AO 0 COM and AO 0; therefore the Glassman power supply is connected to these two ports [28].

On the backside of the Glassman power supply one can manually choose how to operate the instrument depending on how it is connected. Figure 3.8 is an illustration of how the Glassman is connected for this specific project. Ground and Interlock are connected via an emergency stop, which allows for quickly turning off the power supply in case of an accident or emergency, and thus provided the test-set up with an extra safety measure. The DC 0 – 10 V from ADAM-4022T is connected to V-program and Common. The other connections are necessities for the Glassman to be able to operate. [29].

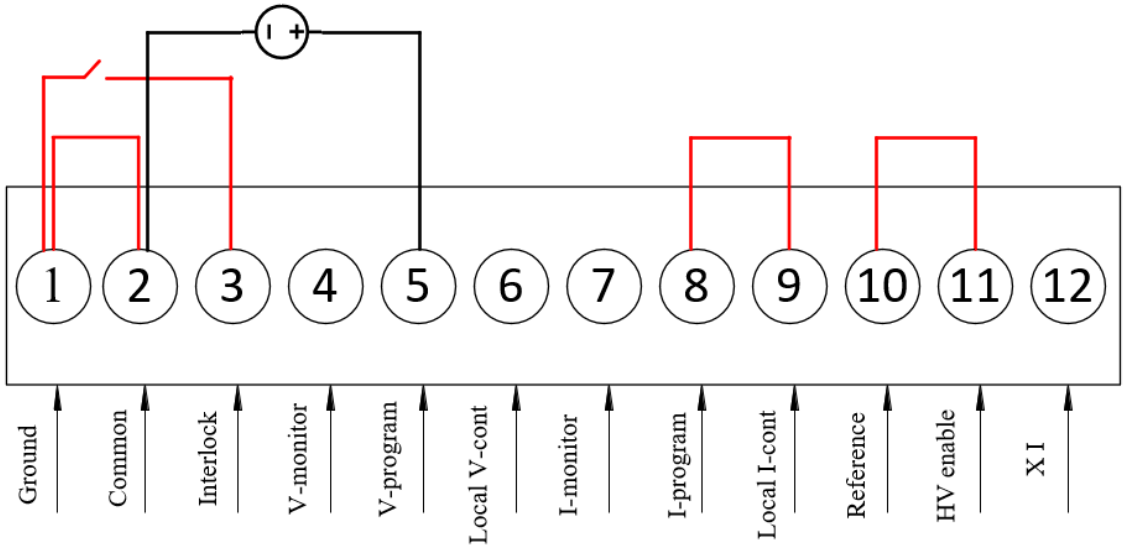

Figure 3.8: Back-side of the Glassman power supply and its different connection points.

3.2.7 Measurements of the current

For this project a Keithley picoammeter 6517B is used, it has a range of ± 10 [aA] to ± 21 [mA] [3]. The Keithley collects and saves data via LabView and communicates with the computer via RS232-USB converter. As mentioned in section 3.2.2 the connection between the test-cell and the Keithley is via a coaxial cable that has been separated such that the copper core goes to the measuring electrode and the shield is connected to the test-cell body and internal guard ring which are grounded. The Keithley operates in a remote mode since it is controlled by the computer via the LabView-program, futher described in section 3.2.8, and runs a current measurement program with an autorange.

3.2.8 LabView-program

A major part in the construction of the test-cell has been to develop a LabView-program to be able to simultaneously control the Glassman power supply and acquire data from the test-cell via the Keithley picoammeter. In the previous sections 3.2.6 and 3.2.7 it has been presented how the Glassman and the Keithley are controlled and operated, and only briefly mentioned that the core of the control is the LabView-program.

The program uses a standard approach usually referred to as a *state machine*, which essentially is a case-structure inside a while loop. The principle of the state machine is that, when a state is finished it moves directly in to the next and continues in the same fashion until it reaches some kind of stop that ends the loop. The state machine in this case consists of eight states:

1. INITIATE, in this state each variable is initiated, in other words the variables are given a value.
2. RAMP UP - 1, here the voltage to the Glassman power supply is ramped to a certain value chosen in the program.
3. CONSTANT - 1, this state keeps the end value of the ramp constant for a certain time that is set in the program.
4. RAMP UP - 2, the voltage is ramped to a second voltage level set in the program.
5. CONSTANT - 2, same principle here as in ”CONSTANT - 1”.
6. RAMP UP - 3, here the voltage is ramped to a third voltage level set in the program.
7. CONSTANT - 3, same principle here as in ”CONSTANT - 1” and ”CONSTANT - 2”. In this state the program also stops when the timer is reached.
8. ERROR, if there occurs and error during the execution of the program it will stop the entire program and lower the voltage to 0V.

The purpose of this program is to allow the user to set three different voltage levels and three different times, at which the program automatically will ramp the voltage and then keep the value at the end of the ramp constant until the set time. It then moves on to the next ramp and continues until it has completed all the set values and set times. How these settings are set can be seen in Figure 3.9 where

an example of test settings are shown. The different times are set at ”Trig - level 1”, ”Trig - level 2” and ”Trig - level 3”. The voltage levels are set at ”Voltage level 1”, ”Voltage level 2” and ”Voltage level 3”, it can also be observed that the voltage is set to 0.74, 1.48 and 2.2 respectively. As mentioned in section 3.2.6 1V output from ADAM-4022T relates to 5 kV output from the Glassman, so these levels are 3.7 kV, 7.4 kV and 11 kV respectively. The increment of the ramp is chosen by setting a suitable value at ”Delta” and a start value is set at ”Start”. Another key point is the ”Command” control at which the user can choose how to operate the Keithley picoammeter, in this case it runs a DC current measuring program and a simple read function. When the program is running each value acquired from the measurement can be observed in real-time at the six different displays depending on what state the program currently is running.

The communication with the ADAM-4022T device, which in turn controls the Glassman, and the Keithley are performed with VISA Write and VISA Read. Since ADAM-4022T only outputs, it will only be in need of VISA Write functions. The Keithley however is a bit more complex since it should operate in a certain way as well as acquire data and save it. It requires VISA Write functions in order to make the Keithley perform current measurements and it then needs VISA Read functions to read the current values. What happens next is that current value from each iteration is then saved into a text file which then can be plotted in for example MATLAB®.

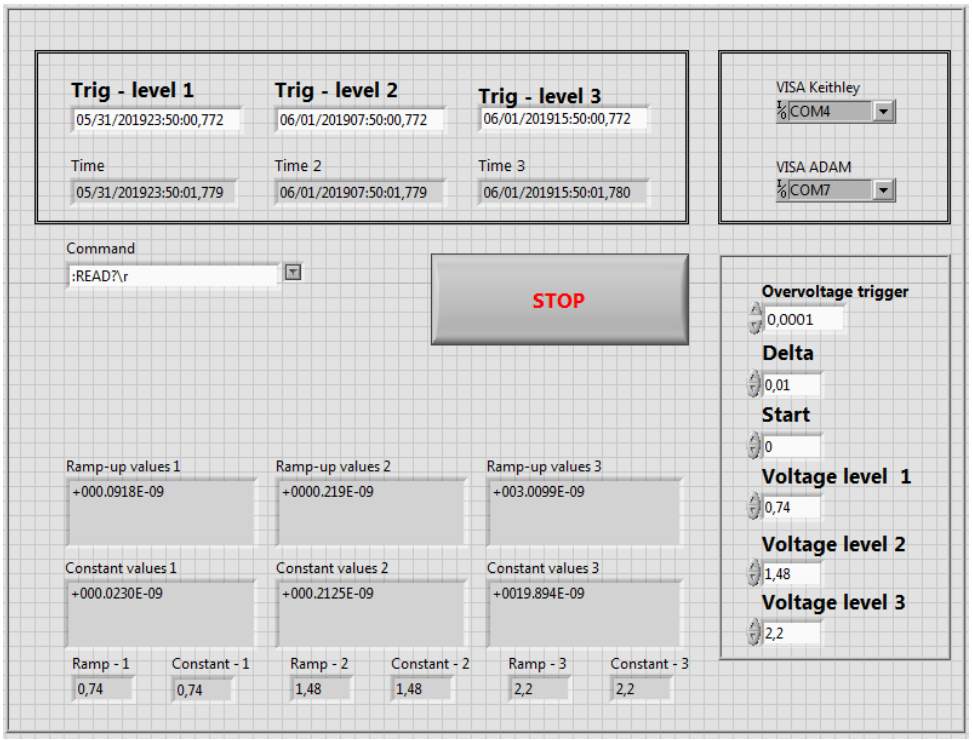

Figure 3.9: This is the graphical user interface of the LabView-program used to control the instruments and acquire data.

3.3 Testing

During the entirety of the Methods chapter it has been thoroughly explained what components are used and how they operate. The details about the tests that are performed on the samples are now described. Each sample (cable peeling and press-molded plate) will be placed in the test-cell, which in turn is located in a heating chamber. Each sample will be tested for a period of 36 hours, this time will be evenly distributed in to three time intervals of 12 hours with three different voltage levels of; 3.7 kV, 7.4 kV and 11 kV. This test will be performed within the heating chamber and with two different temperature levels; 30°C and 70°C. In total there were 6 samples tested, 3 cable peelings of varying thickness and 3 press-molded plates.

A series of tests were performed with TC1, but without anything to compare with it was difficult to determine if it produced reliable and plausible results. In order to ensure this a benchmark between the different test-cells was performed, to see which test-cell presented the best results for these kinds of measurements. The benchmark consisted of two different tests, where only one parameter was changed at a time to ensure clarity in what parameter affects what result. First, the three different test-cells were used for leakage current measurement with voltage levels of 5 kV, 10 kV and 15 kV on an insulation cable peeling. Secondly, the test was repeated with a semiconductor-insulation cable peelings with voltage levels of 2.5 kV, 5 kV and 7.5 kV. The reason for the change in voltage level is because of different insulation thickness of the two samples, which is further elaborated in section 4.4.

4

Results

The results section of this master thesis will contain all the investigations that have been performed for the duration of the project as well as the main measurements of the cable peelings and press-molded plates. It is valuable to present results of the investigations since they might have a significant influence on the conductivity measurements.

4.1 Kapton as film for press-molded plates

There have been studies confirming that the choice of press-film when performing press-molded plates significantly affects the measured conductivity. H. Ghorbani, et. al., conducted measurement using both PET-films and Aluminium-films when creating their press-molded plates. The results showed that there were some strange behaviour when a thermal cycling-test was performed. Except for an overall higher conductivity for the plates manufactured using PET-films, there were also curious peaks during cooling from 70° C and from 90° C down to room temperature.

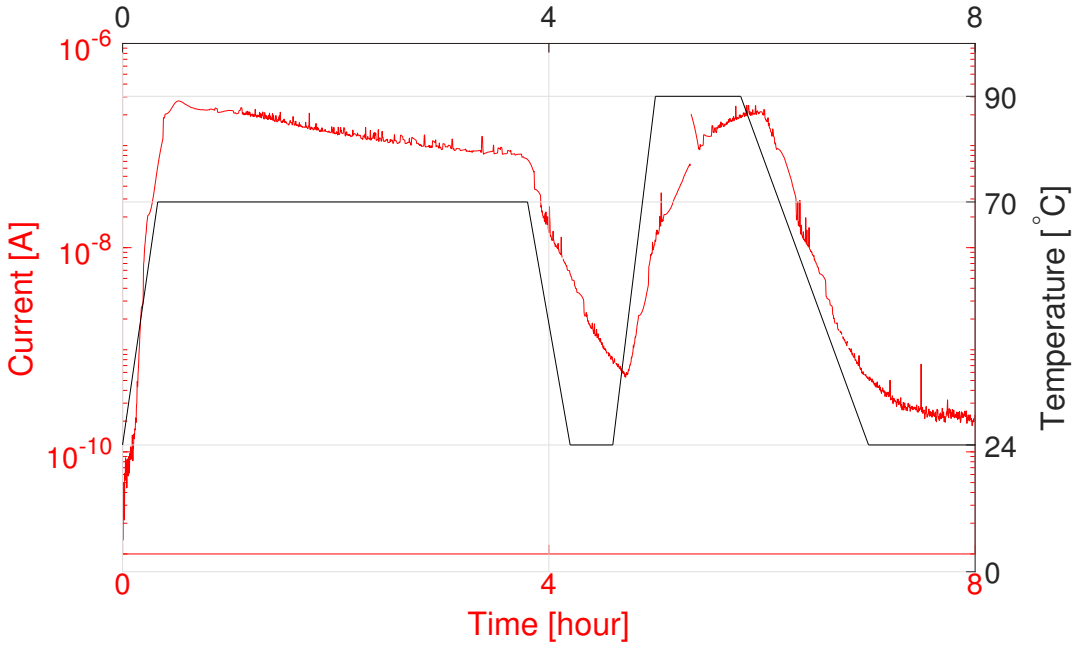

Figure 4.1: Results from temperature cycling test with a press-molded plate manufactured with kapton as press-film, where the temperature cure is an indication of temperature set points and not the actual internal sample temperature.

For this master thesis kapton was used as press-film, as mentioned in section 3.1.2. Since there are no documented effects on conductivity using kapton as press-film, the effects of this pressfilm had to be confirmed by performing similar tests as H. Ghorbani, et. al. The temperature cycling program used is presented in Figure 4.1 and is shorter than that used by H. Ghorbani, et. al., but consists of similar temperature levels, further the electric field strength is chosen to be 30 kV/mm by using an insulation LDPE press-molded plate with a thickness of 0.4 mm and applying a voltage of 12 kV. The results of the temperature cycling is shown in Figure 4.1. It is clear that kapton as press-film does not give the non-monotonic conductivity of the press-molded plate, as no peaks appear during the ramp up or ramp down of temperature. hence the plates that were manufactured for this master thesis at Nexans Norway should not provide any strange peaks in measured leakage current during temperature cycling, and present behaviour that can be represented with equation (2.6).

4.2 Roughness measurements

In this section the results from the optical profilometry measurements of various peeled and press-molded samples will be presented. The aim is to understand and analyse how different roughness of the peeled and press-molded interfaces in contact with the ground electrode, could affect the charge injection from the high voltage electrode and in turn the conductivity.

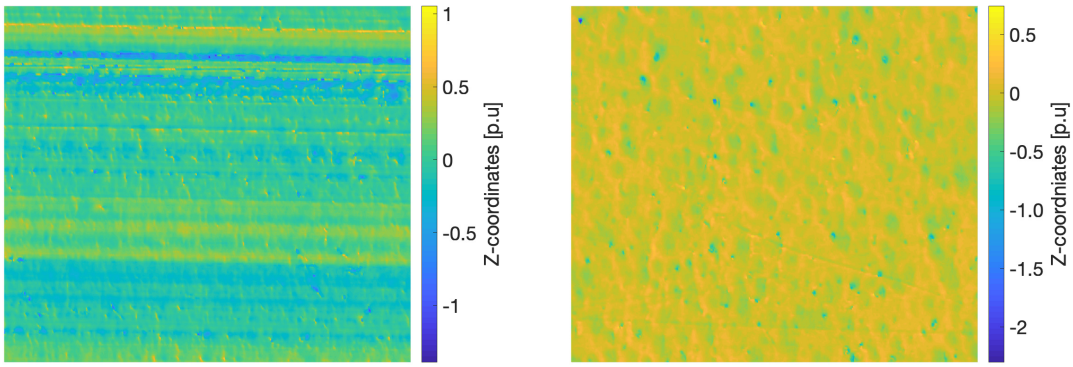

(a) **(b)**

Figure 4.2: Insulation surface scan of a) peeled sample and b) press-molded sample.

In Figure 4.2a and 4.2b the scanned surface of a peeled and press-molded sample can be obtained. The colorbar indicates the peaks and valleys of the sample, where zero p.u means a completely smooth interface. Positive values indicates peaks and negative values valleys. It can be observed that the deviations in surface roughness for cable peeling and press-molded plate are not that different, indicating that the roughness should not affect the conductivity of the two different sample types significantly. In Figure 4.3 the fluctuations of the surfaces are visualised for several

measurements, where the y axis represents the amount of datapoints, and thus the surface fraction, which is located at a specific surface height. An infinitely smooth interface would be represented as a single peak at Z=0, and here we can see the introduced deviations/texture that widens the histogram.

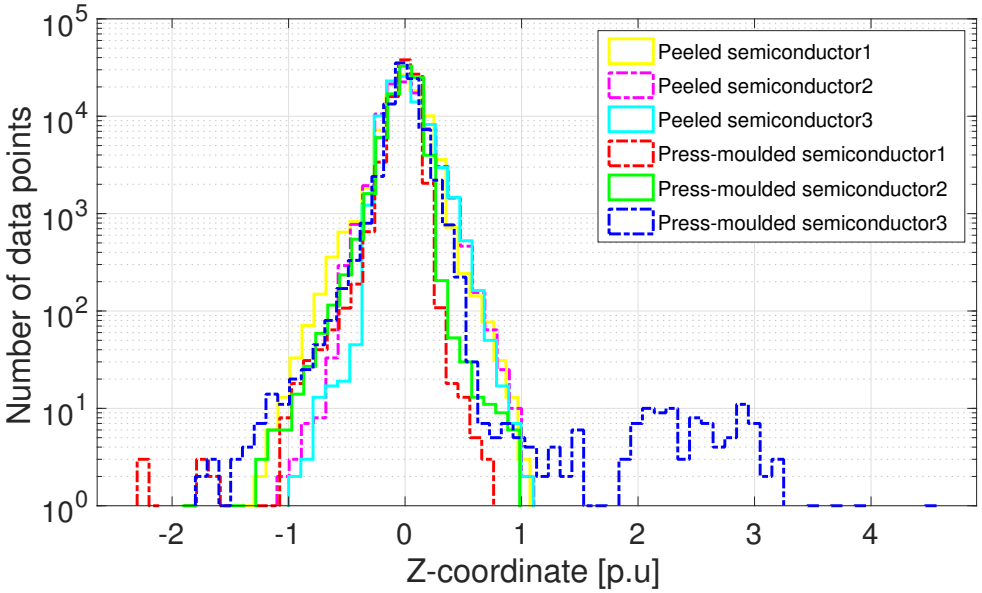

Figure 4.3: Surface height histogram indicating the deviation from the mean height of the surface.

As can be observed from Figure 4.3 the fluctuations follows the same trend as for the cross-sections presented in Figure 4.2a and 4.2b, where the fluctuations are similar for the two sample types. Individual peaks beyond 2 p.u can be overlooked, since it is more likely to be dust on the surface than irregularities of the sample. The fluctuations presented in Figure 4.3 can be integrated through equations 2.7, 2.8, 2.9 and results in the roughness parameters S_a [m], S_q [m] and S_{dq} [deg]. In table 4.1 the normalized values for these parameters are presented and are a numerical indication of the surface roughness.

Table 4.1: S_a, S_q and S_{dq} parameters for the different samples presented in Figure 4.3

Sample	S_a [p.u.]	S_q [p.u.]	S_{dq} [p.u.]
Peeled semiconductor 1	1.714	1.695	1.512
Peeled semiconductor 2	1.773	1.655	1.210
Peeled semiconductor 3	1.654	1.550	1.114
Press-molded semiconductor 1	1	1	1
Press-molded semiconductor 2	1.254	1.223	1.449
Press-molded semiconductor 3	1.252	1.535	2.136

The parameters for S_a and S_q in table 4.1 can be observed as different box plots in Figure 4.4 and 4.5.

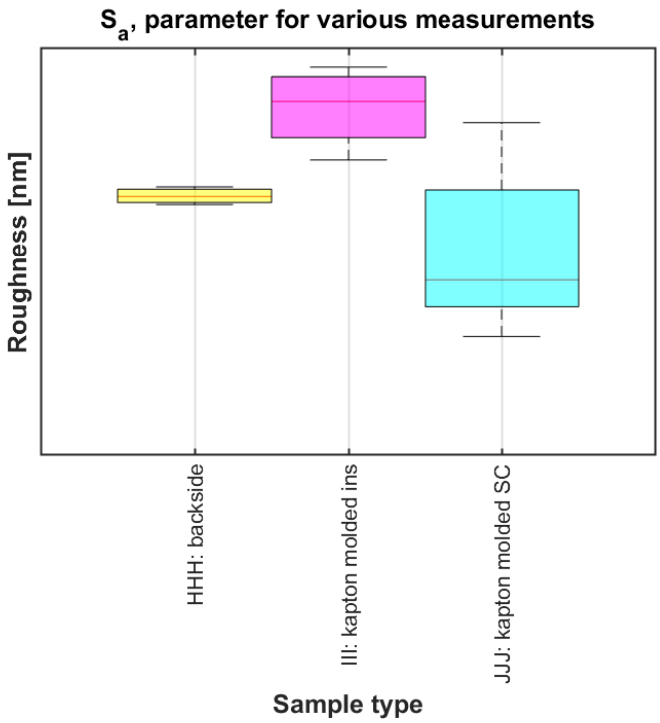

Figure 4.4: Box plot for the S_a parameter for the different interfaces where backside refers to the cable peelings, kapton molded ins and sc to the insulation and semiconductive side of the press-molded plates respectively.

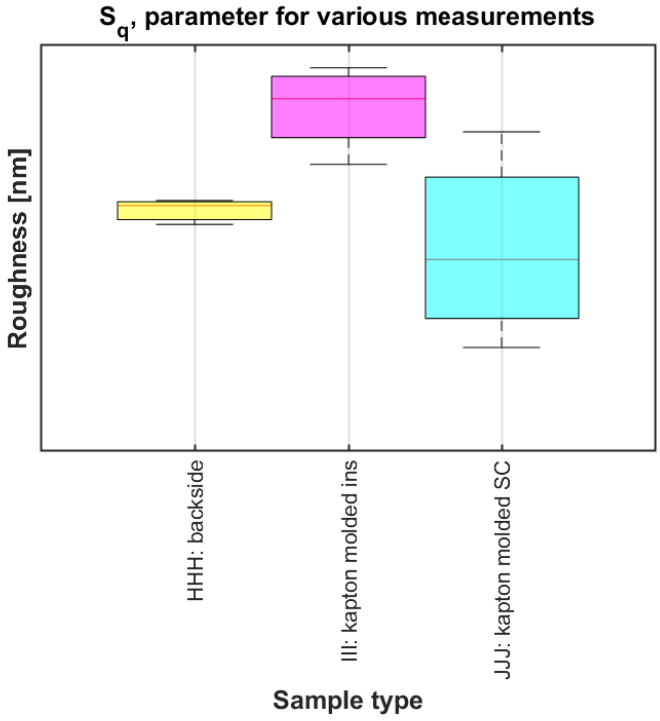

Figure 4.5: Box plot for the S_q parameter for the different interfaces where backside refers to the cable peelings, kapton molded ins and sc to the insulation and semiconductive side of the press-molded plates respectively.

As can be observe from Figures 4.4 and 4.5 the surface roughness of the press-molded insulation interface is added. This in order to present data for the discussion about the manufacturing process of the press-molded samples, in terms of roughness. From the results presented in this section it can be stated that the external surface roughness for the cable peelings and the press-molded plates is similar and relatively low. Indicating that the roughness should not affect the charge injection significantly, in turn not affecting the measured conductivities. The internal insulation-semicon interface was not assessed in this study.

4.3 Cable peeling- and press-molded plate thickness

To be able to determine the electric field strength that the samples have been subjected to, the thickness of the different samples was assessed. This could not be measured by an ordinary measurement tool since it is the thickness of the insulation part that is of significance, since the semiconductor is treated as a conductor when it experiences high voltage. In Table 4.2 the thickness and electric field is presented for all the different samples that were tested. In Figure 4.6 the thickness of a peeled sample, collected from the microscopy, is visualised. Worth mentioning is that the thickness presented in table 4.2 is a mean value from multiple microscope measurements, where the complete study can be found in the Appendix A.

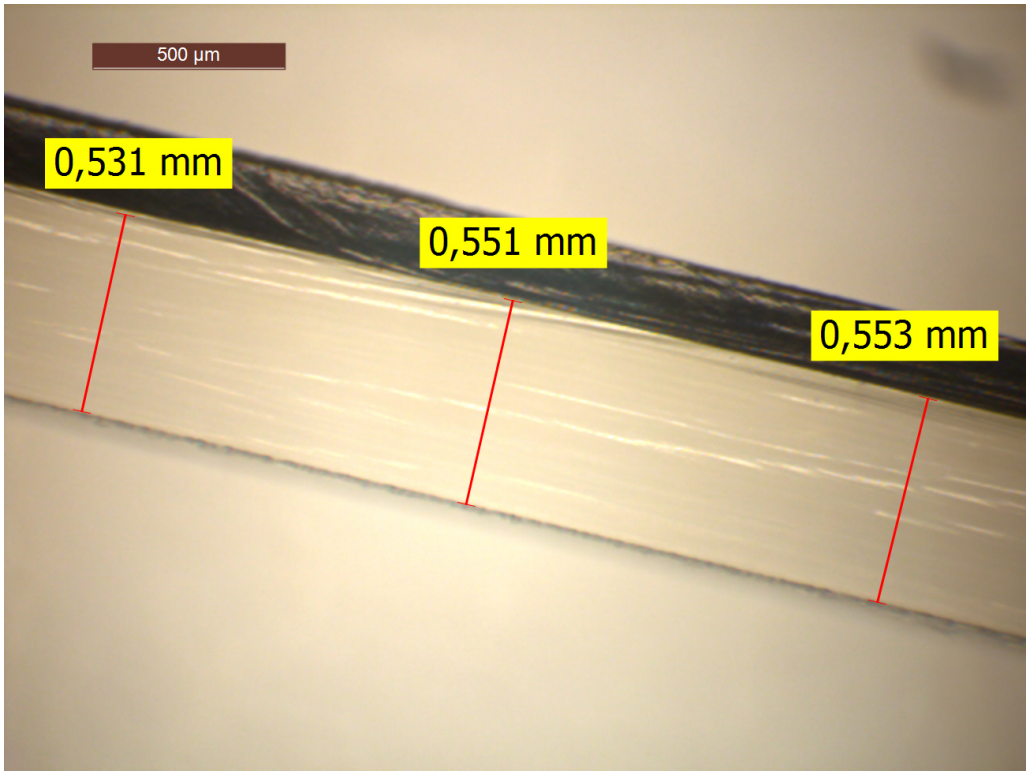

Figure 4.6: One of the cross-sections from the microscopy used to determine the insulation thickness of sample O14.

Table 4.2: All the samples and their respective average thickness, as well as the different electric field depending on the three different voltage levels.

Samples	Mean thickness [mm]	E1 [kV/mm]	E2 [kV/mm]	E3 [kV/mm]
O08	0.40	9.81	18.62	27.68
O11	0.08	48.62	92.24	137.12
O14	0.41	9.59	18.20	27.06
PM1	0.15	26.00	49.33	73.33
PM2	0.20	19.50	37.00	55.00
PM3	0.17	22.94	43.53	64.71

4.4 Benchmarking of test-cells

The results of the benchmark between the different test-cells mentioned in section 3.3 are presented below. In Figure 4.7a, 4.7b and 4.7c the result of measurement of the leakage current measurement on the insulation sample using TC1, TC2 and TC1-G respectively is presented.

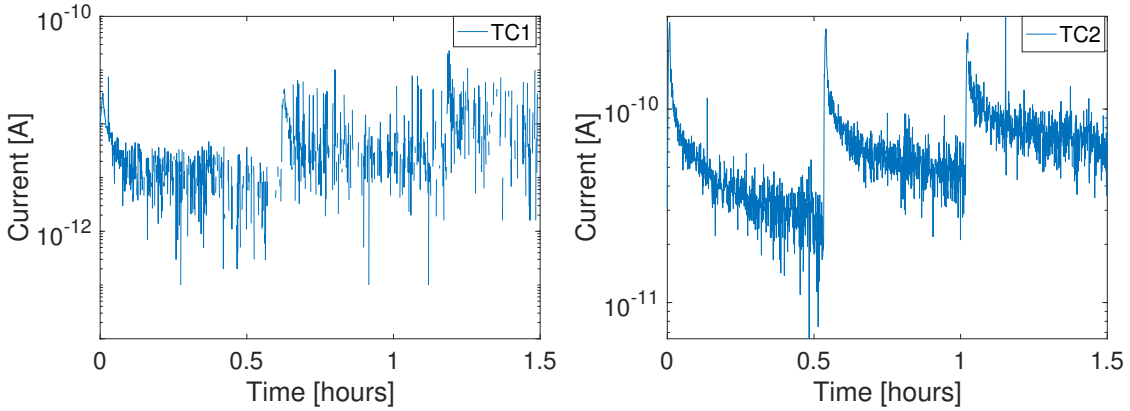

(a)

(b)

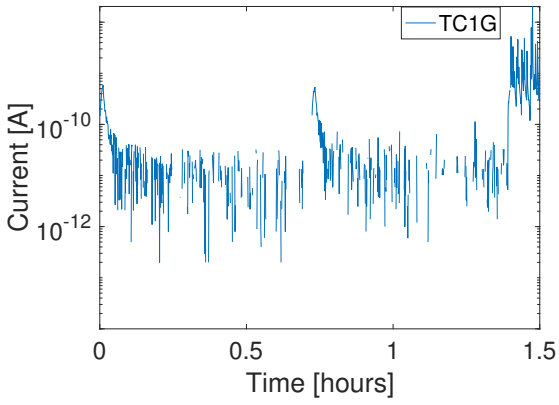

(c)

Figure 4.7: Leakage current measurement of insulation cable peeling using; (a) TC1, (b) TC2 and (c) TC1-G at three different poling voltages.

From the results shown in Figure 4.7a, 4.7b and 4.7c it is clear that all test-cells acquire measurement data that is plausible, as a leakage current of 10^{-10} [A] and below is fully reasonable [30]. However, the measurement performed using TC1 is very inconsistent and the sought shape of the current against increasing voltage levels cannot be fully observed. In Figure 4.7c it can be seen that there is a resemblance of the sought current characteristics, but the result is very unstable. Several data points are missing because of negative values, which are ignored when plotting semi-logarithmic. It is also possible to observe that the test did not run the full 1.5 hours it was supposed to, this is because there were some transients exceeding the limits of the Keithley picoammeter which results in the LabView-program terminating the measurement as a safety precaution. TC1-G provides similar results in regards of inconsistent measurements as TC1, this can be seen in Figure 4.7c. Another similarity with TC1 is that the measurement was terminated due to high transients, these occurred earlier in TC1-G than in TC1. From the results in Figure 4.7b it is clear that TC2 provides the most accurate measurements, which can be seen by the range of the current. In TC2 the current is in a range of 10^{-10} [A] to 10^{-11} [A], and for TC1 as well as TC1-G the range is 10^{-10} [A] to 10^{-12} [A]. It can also be seen that the current-time characteristic is very plausible, this is observed in Figure 4.7b by the significant increase of the current as the voltage increment, and the characteristic current decay as the voltage becomes constant.

The main focus of this project is to compare the semiconductor-insulation interface of a cable peeling and a press-molded plate, hence it is of great importance how well the test-cell measures a sample containing both semiconductor and insulation. Therefore a benchmark was performed using a cable peeling with semiconductor-insulation interface, the results can be observed in Figure 4.8. For these tests using semiconductor-insulation cable peeling the voltage levels were lower compared to the tests performed on the insulation cable peeling. The reason was to avoid a significant effect of the triple point that occurs when a semiconductor-insulation sample is used. Another reason is that the insulation thickness was lower for the semiconductor-insulation peelings compared to the insulation peelings, hence the electric field would be too high if the same voltage was applied. The applied voltage levels were; 2.5 kV, 5 kV, 7.5 kV.

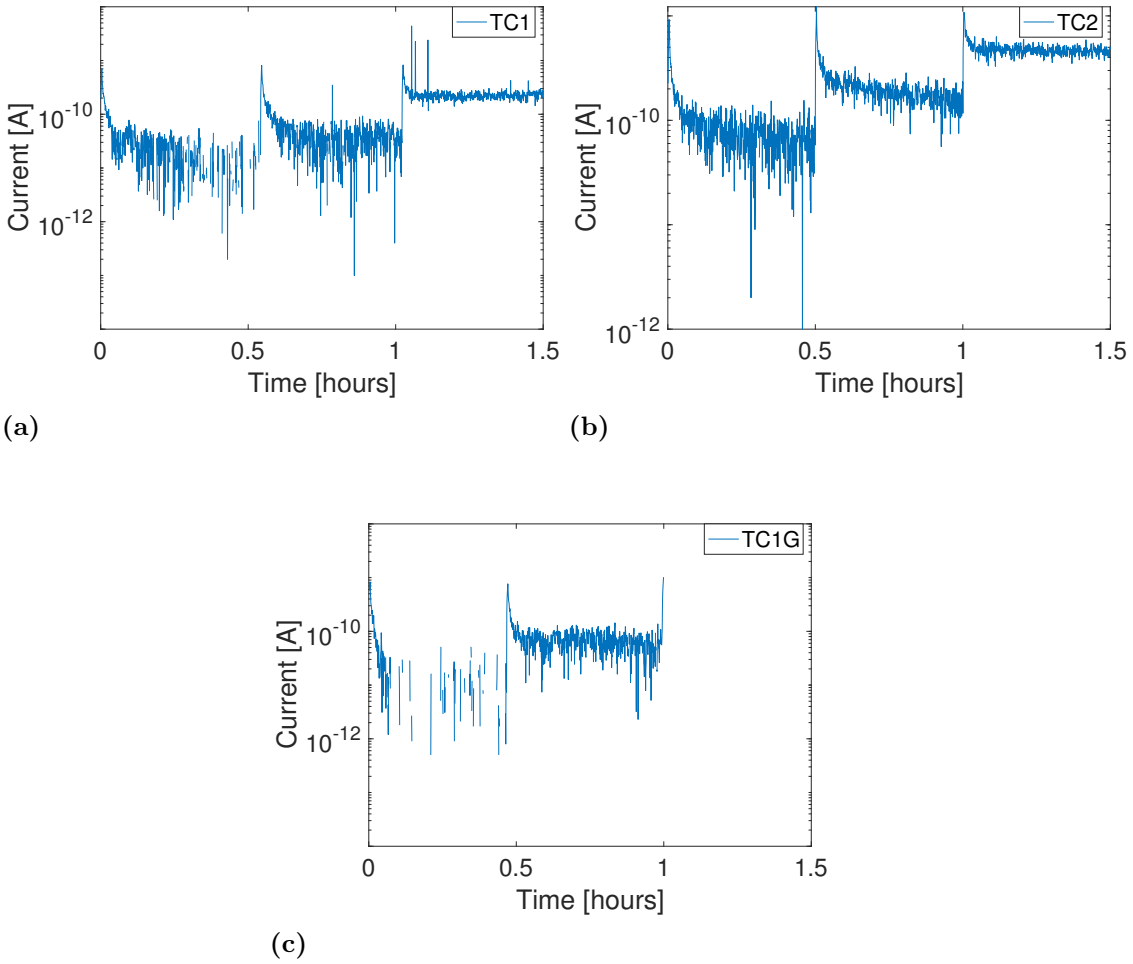

Figure 4.8: Leakage current measurement of semiconductor-insulation cable peeling using; (a) TC1, (b) TC2 and (c) TC1-G.

The benchmark of TC1, TC2 and TC1-G resulted in Figure 4.8. From Figure 4.8a it is observed that TC1 provides quite promising results, compared to its result using a insulation sample. There is a rather high disturbance on the first and second voltage level, but the disturbance on the third level is relatively low. The current characteristic is very plausible as well. In Figure 4.8c the result of the leakage current measurement using TC1-G is presented, it is observed that a lot of measurement data is ignored due to negative values at the first level. At the second voltage level, the current is plausible with respect to both range and characteristic, however as the voltage ramps to the third level the transients become too high and the measurement is terminated. As expected TC2 performs best for a semiconductor-insulation sample as well, which can be seen in Figure 4.8c, and the result seems very plausible. There is a lot of disturbance at the first level, but with the second and third level the disturbance is reduced significantly. This indicates that it will operate well for a higher set of voltage levels. It is clear that it provides the most accurate result using a semiconductor-insulation sample as well, but it was not as significant as with the insulation sample.

From Figures 4.7 and 4.8 it was clear that TC2 is the best suitable test-cell for the leakage current measurements. It is noted in Figure 4.7b and 4.8b that there are some inconsistencies in the measurements. To mitigate these disturbances a DC capacitance was added to the high voltage circuit. Together with the current limiting resistor this forms a low pass filer, with the purpose of reducing the experienced noise. The effect of the DC capacitance is observed in Figure 4.9. The results indicate that the capacitance did not improve the noise level in the leakage current measurements by much. Since the best possible result is desired the capacitance will not be used during further measurements using TC2.

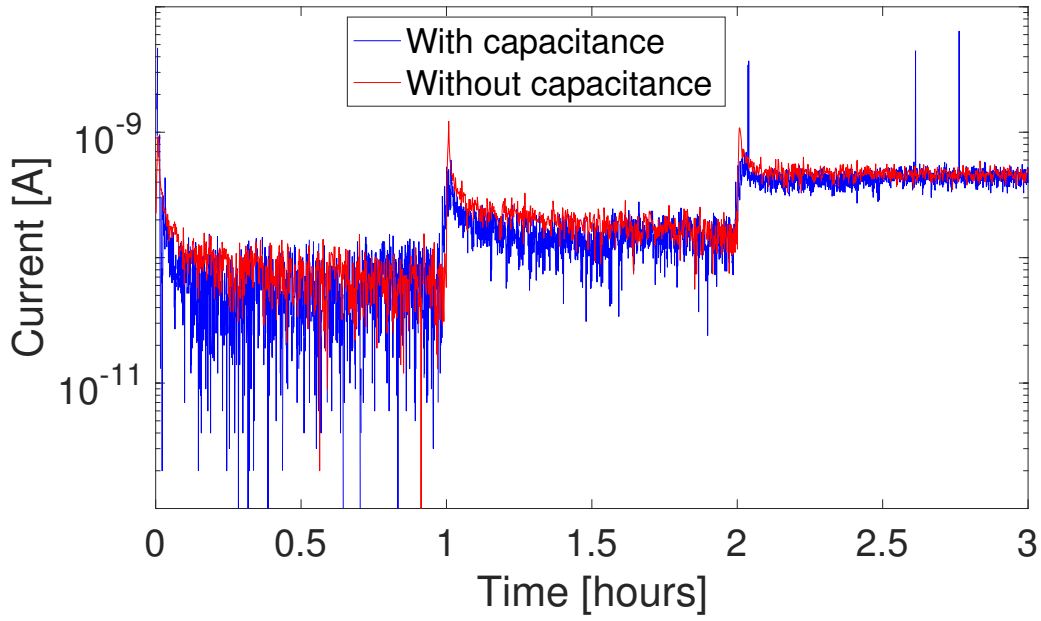

Figure 4.9: Effect of the DC capacitor on the leakage current measurement using TC2.

4.5 Results of conductivity measurements

In this section the results from the conductivity measurements of cable peelings and press-molded plates will be presented. It will begin with section 4.5.1 where the results from the peeling-measurement will be presented and then followed by section 4.5.2 with the press-molded plates. Worth mentioning for this section is that test-cell TC1 was utilised for the conductivity measurements. This because test-cell TC2 behaved strangely for the longer testing procedures, which was overlooked in the benchmarking tests. This is further elaborated in the discussion of the report.

4.5.1 Cable peelings

There was a lot of minor testing performed during the development, construction and feasibility-testing of the test-cell. However, in this section only the final results will be presented. In Figure 4.10 an example of the current is observed, this test is the peeled sample O08 with the climate chamber set to 70°C.

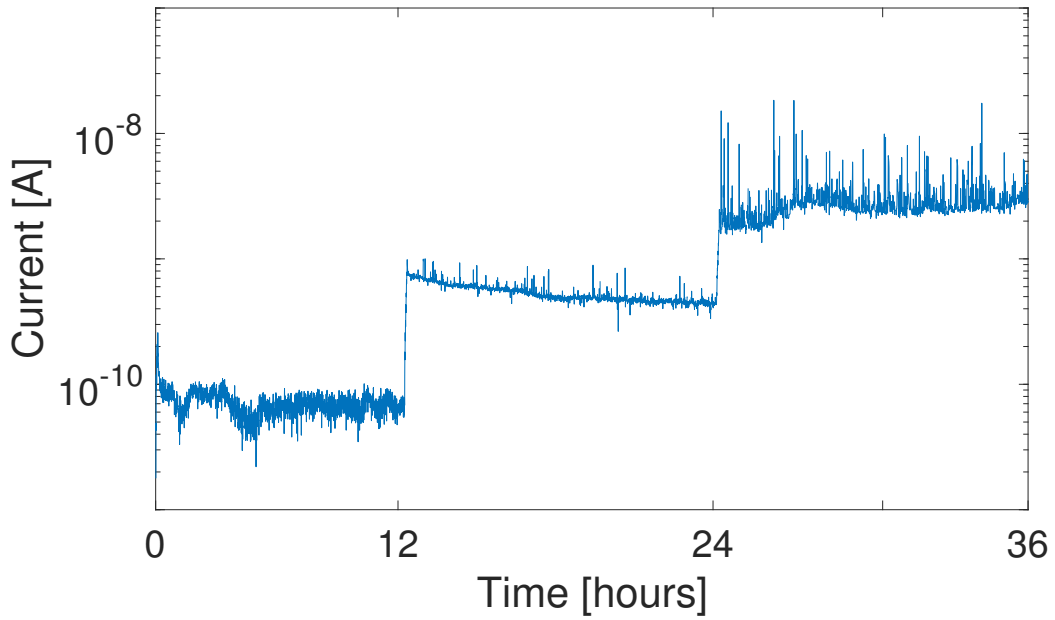

Figure 4.10: Measurement data for peeled sample O08 during 70°C with test-cell TC1 at voltage levels 3.7, 7.4 and 11 kV.

Since current is measured by the test-cell the acquired data has to be processed in order to determine the conductivity, as was shown in equation (2.1) where J and E denotes the current density and electric field respectively. To avoid an unnecessary amount of plots in the result section the measured data for the different sample are instead presented in Table 4.3. Where the steady state value, reached after 12 hours, from each voltage level is taken and converted to conductivity.

Table 4.3: Measurement values of current and conductivity for the peeled samples after 12 hours.

	30°C			70°C		
	3.7 kV	7.4 kV	11 kV	3.7 kV	7.4 kV	11 kV
Sample	**Current [A]**					
O08	1.26E-12 (?)	1.80E-12	3.71E-11	6.49E-11	4.17E-10	3.05E-09
O11	NaN	NaN	NaN	NaN	NaN	NaN
O14	1.17E-12	1.51E-12	3.63E-12	3.34E-11	1.83E-10	1.95E-08
Sample	**Conductivity [S/m]**					
O08	1.9E-16	1.4E-16	1.91E-15	1.0E-14	3.2E-14	1.57E-13
O11	NaN	NaN	NaN	NaN	NaN	NaN
O14	1.8E-16	1.2E-16	1.9E-16	5E-16	1.4E-14	1.03E-12

In table 4.3 it can be observed that a question mark follows one of the measurement values, the (?) indicates that there were uncertainties when acquiring the data and the reliability is questionable. The NaN (Not a Number) notification implies that there were no successful measurements conducted from the specific sample. From equation (2.5), presented in section 2.2, the bulk-conductivity for the specimen can be observed. In the formula the constants σ_0, α and β are used to numerically match the measured conductivity. In Figure 4.11 only the steady state conductivity is presented, together with the fitted line according to Klein's conductivity expression.

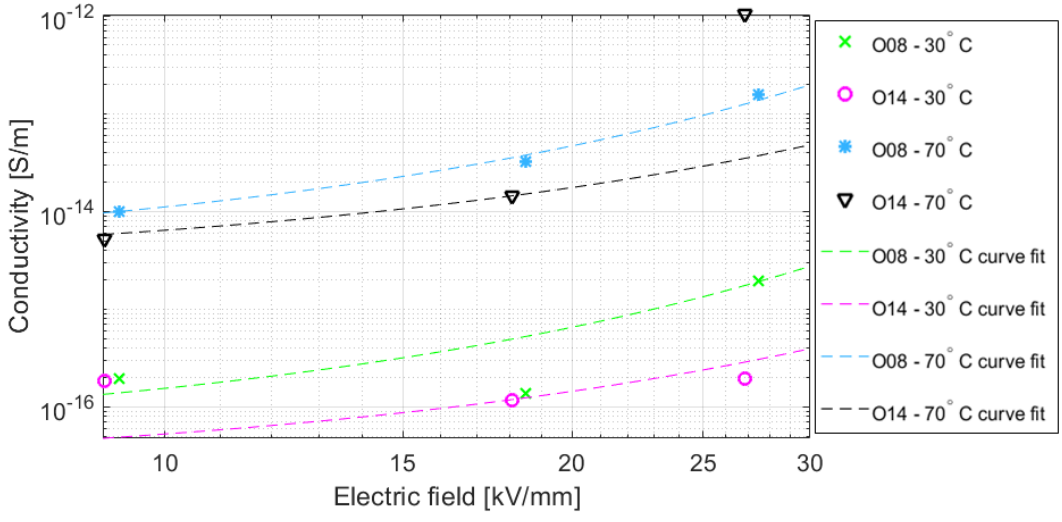

Figure 4.11: One data point from each field level for the cable peelings is plotted and the lines represent an exponential fit of the data points.

4.5.2 Press-molded plates

The result from the conductivity measurement for the press-molded plates are presented similarly as the cable peelings and can be observed in Table 4.4. In Figure 4.12 an example of the current measurement for press-molded plate #1 during 70°C is presented.

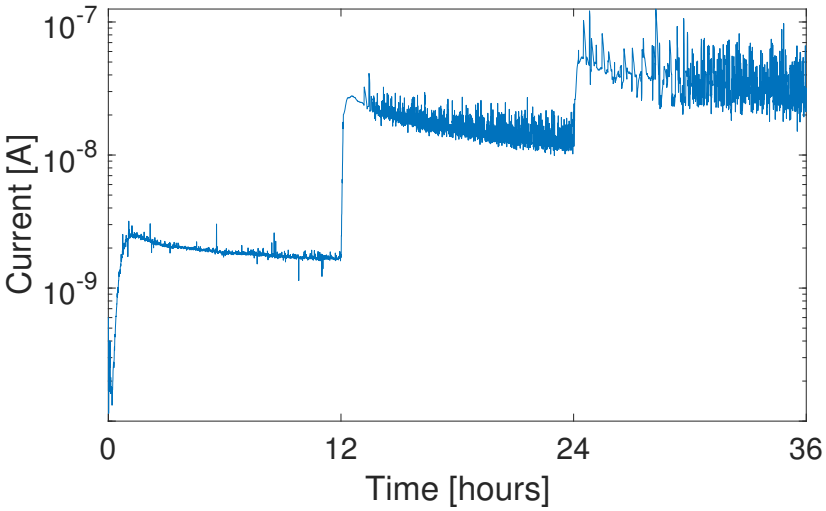

Figure 4.12: Measurement data for press-molded plate #1 during 70°C with test-cell TC1 at voltage levels 3.7, 7.4 and 11 kV.

In table 4.4 the values of conductivity and current for the press-molded samples are presented. The values are derived in the same fashion as for the peeled samples. In Figure 4.13 one data point of the conductivity for each field level, together with the fitted line of the bulk-conductivity can be observed.

Table 4.4: Measurement values of current and conductivity for the press-molded samples after 12 hours.

	30°C			70°C		
	3.7 kV	7.8 kV	11 kV	3.7 kV	7.4 kV	11 kV
Sample		**Current [A]**				
PM1	3.80E-11 (⋆)	1.08E-10 (⋆)	6.19E-10	1.68E-09	1.29E-08	3.14E-08
PM2	1.9E-11 (⋆)	5.45E-11	NaN	3.92E-10	5.43E-09	2.44E-08
PM3	NaN	NaN	NaN	NaN	NaN	NaN
Sample		**Conductivity [S/m]**				
PM1	2.18E-15	3.1E-15	1.19E-14	9.6E-14	3.7E-13	6.05E-13
PM2	1.45E-15	2.08E-15	NaN	3.0E-14	2.08E-13	6.28E-13
PM3	NaN	NaN	NaN	NaN	NaN	NaN

In table 4.4 it can be observed that a star follows some of the measurement values. The ⋆ indicates that there was high noise when the value of the current was acquired. The NaN (Not a Number) notification implies that there were no successful readings for the specific sample.

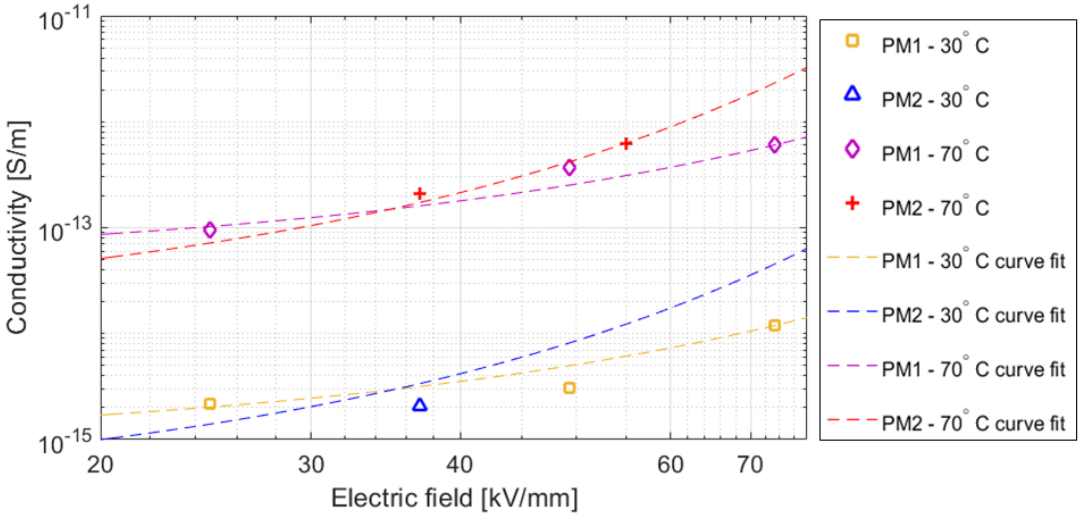

Figure 4.13: One data point from each field level for the press-molded plates is plotted and the lines represent the fit of the conductivity equation to the data points.

With help of the curve fits from Figure 4.11 and 4.13 the parameters α, β and σ_0 from the bulk-conductivity in equation (2.5) could be determined. This was done by using MATLAB™ and its curve fitting algorithm in order to find the optimized fit to the measured data. These values can be further observed in Table 4.5.

Table 4.5: The values of α, β and σ_0 for each sample.

Sample	α $[1/(°C)]$	β $[(kV/mm)^{-1}]$	σ_0
O08	0.1068	0.1438	1.485E-18
O11	NaN	NaN	NaN
O14	0.1200	0.1005	5.254E-19
PM1	0.0981	0.0365	4.327E-17
PM2	0.0984	0.0716	1.246E-17
PM3	NaN	NaN	NaN

While these parameters do show significantly different behaviour between the sample types (i.e. stronger field and temperature dependency for the peeled samples), further aspects must be considered as further discussed upon in section 5.2.

5

Conclusion

In this section the results will be summarised and discussed. Several small scale tests were performed during the master thesis duration, which will be discussed briefly to address the effect they can have on the main measurements. The main focus on the discussion and conclusion is to give an answer to the project aim; is there a difference between the conductivity of a cable peeling sample and a press-molded sample?

5.1 Discussion

After finalising the test set-up, with a reliable program for the data communication, several test series were performed. First, a benchmark of the three test-cells was performed to determine which was more suitable to measure the leakage current of the semiconductor-insulation interface, which is further elaborated upon in 3.2.2 and 3.2.3. During this benchmark it was discovered that performing tests on the chosen interface was rather difficult. The most significant reason for this, according to our analysis, could be the enhanced field that occurs due to the sharp transition at the sample edge which we shall refer to as the triple point. Here the semiconductor edge, being on HV potential, features a sharp edge. The enhanced field at the triple point could have resulted in high noise levels, which was observed from the figures in the result section, since it disturbed the signal from the measuring electrode. When performing conductivity measurements and the applied voltage exceeded 12,5 kV, partial discharges (PD) could be observed and recorded with an ultrasonic translator. In the event of PDs, the measured current increased rapidly and the over-current protection turned off the applied voltage.

In Figure 5.1 the cross-section of each test-cell can be observed, where 5.1a is TC1-G, 5.1b TC1 and 5.1c TC2. The field distribution for TC1-G and TC1 is presented in Figure 5.2a and 5.2b. TC2 will have a similar equipotential distribution as TC1 since it does not have a secondary HV guard ring. It is important to observe that the illustrations are not in scale and that D >> t for the dimensions indicated in Figure 5.2.

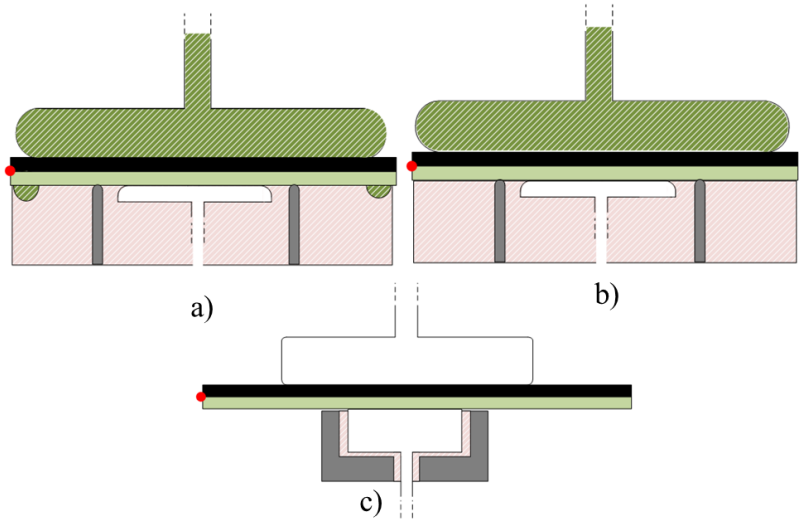

Figure 5.1: The three different test-cells with the triple point marked as a red dot.

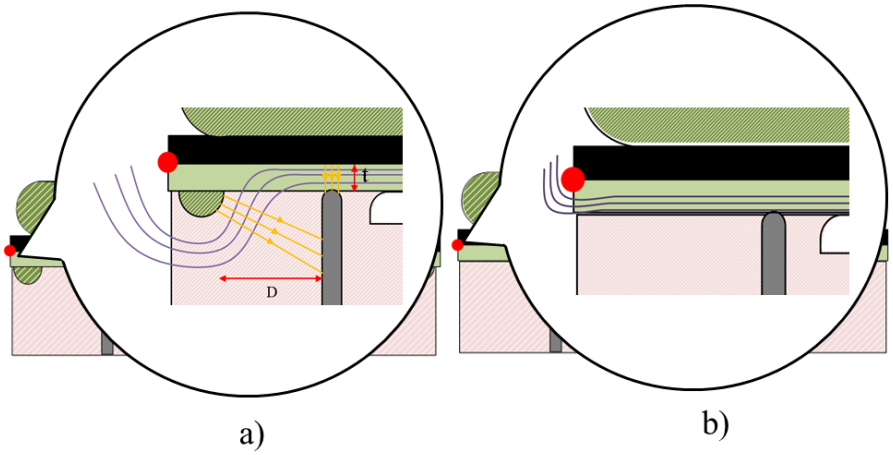

Figure 5.2: TC1-G and TC1 with the equipotential lines and the electric field distribution.

In the construction of TC1 and TC2 the creepage distance, together with the shielding, was assumed to be enough in order to reduce the influence from the enhanced field point. The measurements performed in these cells were highly impacted from noise, which can be observed in the result section. In test-cell TC1-G, this problem was accounted for and a secondary guard-ring was implemented, shielding the triple point. The guard-ring is at the same potential as the high voltage electrode, which will ”push away” the equipotential lines and thus relieve the triple point from en-

hanced electric field. This can be observed in Figure 5.2a, where the yellow lines are the electric field which are perpendicular to the equipotential lines. When comparing the results from the different cells, we could not see the correlation that the noise level was reduced when using TC1-G. This can be due to flaws in the construction and that the distance towards the measuring electrode was not adequate to reduce the impact of the enhanced field point.

In section 4.4 an extensive comparison between the three different test-cells available for this master thesis was performed. This was done to confirm which test-cell provided the most reliable and plausible results. It was determined that TC2 was most suitable for the conductivity measurements of the acquired samples, however once the real long time measurements started, strange results were obtained. It seemed as only noise was recorded. This was very strange and several more test were performed, but with the same result. An example of one of these measurements is presented in Figure 5.3. These observations resulted in that TC1 was selected for the final testing, which made us deviate from the benchmarking. From Figure 4.10 and 4.12 it can be observed that test-cell TC1 performed better for the semiconductor- insulation interface during a longer testing interval. In section 2.2.5 it is concluded that the contact pressure applied to the sample impacts the conductivity. During the benchmarking a specific constant pressure of the sample was sought and for that pressure it was concluded that test-cell TC2 was most suitable for the finial testing. The characteristics of the measured current, presented in Figure 5.3, forced us to make changes in order to increase the reliability of the measurements. Therefore, the pressure which the sample was subjected to was increased and the calibration presented in section 3.2.5 was overlooked. With a higher pressure it was concluded that test-cell TC1 operated most efficiently and further indicates that the pressure impacts the leakage current, by improving the mating quality with the ground electrode. These changes resulted in an unknown pressure, in terms of quantity, for the finial testing. This increased pressure level was used consistently for all the measurements presented in the result section.

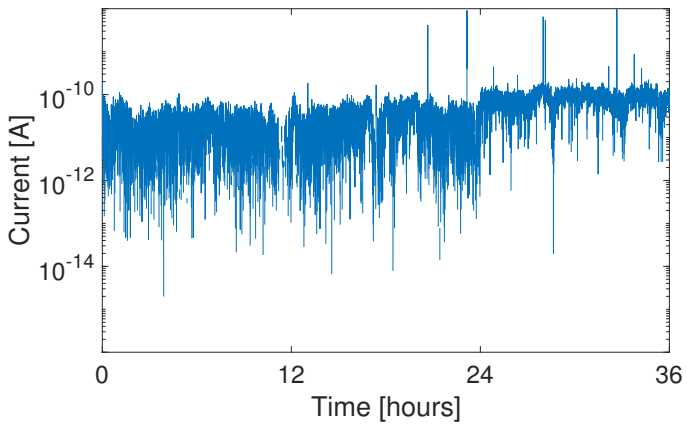

Figure 5.3: Example of noisy measurement using TC2 for a longer measurement at voltage 2.5, 5 and 7.5 kV.

In section 2.2.4 it has been stated that temperatures close to T_m can change the rate of crystallisation within the specimen. The peelings used for the electrical testing are degassed during the manufacturing of the full size HVDC cable, while the material used for the press-molded samples is not. In order to achieve similar impurity content of the peelings and the press-molded samples, the degassing time for the press-molded samples were chosen to be longer than for the peelings. The time for the degassing process could in turn affect the conductivity and make the comparison imperfect. Since part of this project was to analyse the correlation between conductivity and temperature, the samples were subjected to a third reheating process during the electrical testing. The highest testing level, 70 degrees, is the same temperature that was chosen for the degassing procedure and the duration of the testing corresponds to the degassing time. This means that each tested sample was exposed to at least one experiment, while some samples needed to be tested several times, during which the crystallinity of the specimen could change and further outgassing could occur. It can however be postulated that the majority of the byproducts from the manufacturing was eliminated during the degassing process. The rate of the crystallisation is on the other hand an uncertainty for the results of the conductivity measurements.

From the results presented in table 4.4 it can be observed that there are no values presented for press-molded sample #3. This is because all tests that were performed on this specific sample resulted in the triggering of the over-current protection. The explanation for this is likely due to errors during the manufacturing process of the press-molded sample and not regarding issues with the chosen test-cell. This resulted in a semiconductor-insulation interface inside the sample #3 that differed from the other constructed samples and in turn made this measurement invalid. But fortunately, there was only one sample that consistently showed strange behaviour for the leakage current measurement. From table 4.4 it can also be observed that press-molded sample #2 is lacking data for 11kV and 30°. The reason for this is that the over-current protection was activated for this level, but the problem in this case was probably due to high noise levels that made the measured current oscillate to the extent were the protection triggered. In table 4.4 it can be observed that press-molded sample #2 is missing data on the third voltage level at 30°, probably due to some error with the measurements.

From table 4.3 it can be observed that peeled sample O11 is lacking measurement values, all tests performed on this specific sample shut down due to the over-current protection of the LabView-program. The reason for this is likely due to the varying thickness of the sample and can be observed from Figure A.3 in Appendix. The smallest thickness that was recorded for this sample was around 0.04 mm, which meant that the electric field in that point became 275 [kV/mm] for the highest voltage level. Since the over-current protection triggered during the testing it indicated that the thin insulation of the sample was not enough to separate the high voltage from the measuring electrode and a breakdown might have occurred in the sample.

In section 2.2.2 the underlying theory of the bulk conduction was presented and in equation (2.5) the temperature dependency is derived. From the results of the conductivity measurements it can be observed that the readings from the peeled and molded samples, presented in Table 4.3, correlates with the theory and indicates reasonable measurement results. A comparison between cable peelings and press-molded plates could therefore be accomplished. The difficulty of producing cable peelings with 0.2 mm insulation thickness, lead to fewer comparable results. In Table 4.2 it was concluded that the electric field strength for the two sample types varied a lot which made it hard to make a comparison between them. However, it can be seen that there are data for both cable peeling and press-molded plate at ≈ 25 kV/mm. This means that PM1 can be compared with O08 and O14. From Figure 3.1 and 4.11 it can be concluded that there is a difference of approximately one decade of conductivity for the two samples at ≈ 25 kV/mm. It is hard to determine what causes this difference. However, three theories can be postulated:

The first hypothesis is that the conductivity is affected by the interface-to-bulk ratio, since the thickness of the samples were not similar. A thicker sample could therefore be more capable of building up a significant homocharge density, in turn leading to a lower leakage current in the sample. The peelings had nearly twice the thickness than that of the plate, meaning that the interface-to-bulk ratio would be completely different. While such a difference is not predicted from the macroscopic bulk conductivity equation, when considering that conduction involves injection, hopping, trapping and detrapping such an effect is viable. In a narrower sample there will be less volume available for electric field reversal caused by the charge distribution, thus giving different behaviour.

The second hypothesis is that the manufacturing process for the two sample types are different which results in that the semiconductor-insulation interface is dissimilar as well. This could affect the charge injection as mentioned in 2.2.5, as different roughness levels or different state distributions might be present at the interface.

The third hypothesis is that the molecular structure of the cable peeling and the press-molded plate could affect the electrical conductivity. The main difference between the two sample types is that the peeling is taken from a full scale cable, which means that the polymer chains might be more oriented than what they are in a press-molded plate since it is not extruded. This was further elaborated in section 2.1.1 and Figure 2.4, where it was stated that a more oriented structure would decrease the conductivity. This is what is observed from our measurements as well; the conductivity is one decade lower for the cable peeling compared to the press-molded plate at ≈ 25 kV/mm.

The uniqueness of this thesis is the semiconductor-insulation interface, measurements on a cable peeling or press-molded plate containing this interface is uncommon. This makes it hard to evaluate the results in this thesis against other studies from litterature, however there are several conductivity studies of XLPE press-molded plates that could be used to validate the acquired results in this project. In H. Ghorbani's PhD thesis several studies regarding XLPE insulation were conducted, among them DC conductivity measurements. It was observed that press-molded plates with a thickness of 1 mm using PET as press-film resulted in a conductivity in the range of [fS/m]. These results were acquired with a temperature of 50° C and a field level of 18 kV/mm. These values corresponds very well with the results acquired by the measurement performed on cable peelings and press-molded plates with both semiconductor and insulation. Intuitively an exact comparison cannot be made since the test conditions are not the same, for example both the field strength and the temperature differ from the test performed by H. Ghorbani. The main difference is of course the interface, however the comparison is still of interest to show that the results of semiconductor-insulation cable peelings and press-molded plates is still in an reasonable range of what an insulation press-molded plate is.

In Figure 4.1 in section 4.1 it was clear that kapton is acceptable as press-film material and will not provide strange peaks in conductivity measurements performed during a temperature cycling. The results obtained in the test corresponds well to H. Ghorbani's, et. al., which further strengthens the claim that kapton will not give current transients. However, as it is stated by Ghorbani these peculiar peaks in leakage current occur during cooling from a high temperature to room temperature (in this master thesis as well as in Ghorbani's case from 70°C and 90° to room temperature). This further means that in this master thesis this phenomena would not be a problem even if kapton-film would show similar signs as PET-film since there were no temperature cycling performed during the tests. The temperature was kept constant for the entirety of the conductivity measurements and instead the voltage was dynamic with three different voltage levels. Even though it was expected that this phenomena would not affect the measurement results significantly, confirming transient free conductivity performance indicates that there are likely no impurities originating from the press film, which would cause such a phenomenon.

5.2 Conclusion

The aim of the master thesis consisted of two parts; construct a leakage current testing set-up for investigation of the semi-conductor-insulation interface of an HVDC-cable and determine if there is a significant difference between the conductivity of press-molded plates and cable peelings.

The testing-set up was successfully constructed and operated as expected, for 30°C the leakage current was very low and close to the limit of what the picoammeter could measure, this resulted in a lot of disturbances for some measurements. For 70°C the current was higher which lead to more stable measurements.

If there was a difference in measured conductivity between the two sample types is not easily answered. There was a difference as can be seen in the acquired results, if this variation comes from the difference in sample type or something else is unknown. A lot of parameters vary for the cable peelings and press-molded plates, the overall geometry is one example and leads to different electric field levels due to varying thickness across the sample. This would of course be the case if only cable peelings or press-molded plates would be tested, there will always be difference in thickness since the process of manufacturing both sample types is not fully precise. Further, the microscope studies also confirmed that the electric field strength was different for the two sample types. To be able to make a full comparison the field levels should be the same. It was observed that there was one decade difference in electrical conductivity between peeling and press-molded plate at ≈ 25 kV/mm, the reason for this is unknown but three hypotheses were formulated. It could be due to the difference in interface-to-bulk ratio between the two samples, due to the dissimilar thickness. The second hypothesis postulates that the different nature of the internal semiconductor-insulation interface might affect the results. The third hypothesis postulates that the different morphology is the main cause for the discrepancy, since the peelings are extruded and the plates are not. Literature have provided information that a more oriented molecular structure would lead to a lower conductivity, which the acquired results indicates. Overall, the measurements of the two samples types were in similar range as other studies, hence concluding that cable peelings should be a valid sample to perform testing on to determine electrical characteristics of an HVDC-cable.

6
Future work

There is much more to be studied in this field, as this thesis merely grasped on the conductivity impact including the insulation-semiconductor interface has. Therefore, in this section, some thoughts on what could be improved in the thesis along with studies that were left untouched are presented.

6.1 Roughness measurements

During this projected it is stated that the roughness of the surface might impact the conductivity measurements, but this conclusion is solely based on other projects and their results. For future work a separate study about how the roughness of the semiconductor-insulation interface impacts the conductivity could be performed. This could increase the scientific value and could validate if measurements from the test set-up match the results from other studies. In order to perform these kinds of measurements the surface of the internal semiconductor-insulation interface could be modified with the focus of increasing the roughness, prior to mating it with the insulation plate in the molding process. This could be done with simple sandpaper or a more advanced method. The roughness of the abraded semiconductor could then be measured through an optical profilometry analysis and the adjusted surface parameters could be certified. The abraded samples should then go through the same electrical testing procedure as presented in the report and a comparison could be accomplished.

6.2 Noise levels

To ensure more reliable measurements for future analyses, the noise level within the test cell could be reduced. This could be done with better shielding around the electrode, or by constructing a new test cell were the contribution from the enhanced triple field point were reduced to a wider extent. However, this would require wider samples, which for the peeling method are practically not feasible to manufacture. One could perform further electrical testing, with the focus on analysing how the test-cell behaves with the semiconductor connected to the high voltage electrode and then step by step reduce the impact. The noise that comes from the usage of regular coaxial-cables was an uncertainty for this project and nothing that was taken into account. For future analysis solutions for reducing this noise could be developed to guarantee less noisy measurements.

6.3 Byproduct measurement

In the comparison between the peeled and press-molded samples, focus was put on electrically analysing the different specimens. For future analyses further tests could be performed, which could asses the amount of chemical residues in the peeled and press-molded specimen. Their levels could be controlled to match levels of real cable applications, to confirm that any trends observed in the conductivity measurements prevail even at higher impurity contents. In the study here, this factor was mainly controlled by keeping these residues as low as possible.

6.4 Cable peelings and press-molded plates

For this master thesis several cable peelings and press-molded plats were manufactured. However as the project prolonged there was soon a realisation that more samples were needed. The benefit of having a larger quantity of samples is that more ”virgin”-testing could be performed, which essentially means that all samples were only used once. Re-using samples could lead to accumulation of charges within which could affect the conductivity once the sample was used again. Then all test cell validation testing could be performed on samples that later would not be re-used.

A future study that could be of interest is a list of what materials as press-film will not affect the conductivity of XLPE press-molded plates. Aluminium and PET are commonly used, but PET is documented as unsuitable for press-film as it leaves contaminants in the XLPE that affects the leakage current during temperature cycling Such a study could provide security in which press-films are suitable for conductivity measurements and which are not.

Bibliography

[1] E. E. Peschke and R. v. Olshausen, *Cable systems for high and extra-high voltage : development, manufacture, testing, installation and operation of cables and their accessories*. Publicis MCD Vlg, 1999.

[2] E. Doedens, "Characterization of Different Interface Types for HVDC Extruded Cable Applications," Ph.D. dissertation, 2018. [Online]. Available: https://research.chalmers.se/publication/502706

[3] Tektronix, "Model 6517B Electrometer Reference Manual," Tech. Rep., 2016. [Online]. Available: https://www.tek.com/keithley-low-level-sensitive-and-specialty-instruments/keithley-high-resistance-low-current-electr-0

[4] T. Worzyk, *Submarine power cables : design, installation, repair, environmental aspects*. Springer, 2009.

[5] "Fundamentals of HVDC Cable Transmission," in *Extruded Cables For High-Voltage Direct-Current Transmission*. Hoboken, New Jersey: John Wiley & Sons, Inc., 6 2013, pp. 11–40. [Online]. Available: http://doi.wiley.com/10.1002/9781118590423.ch02

[6] T. Worzyk, *Submarine Power Cables*, ser. Power Systems. Berlin, Heidelberg: Springer Berlin Heidelberg, 2009.

[7] R. Ross and W. Geurts, "Application of polyethylene sheath and swelling powder against water treeing," in *ICSD'98. Proceedings of the 1998 IEEE 6th International Conference on Conduction and Breakdown in Solid Dielectrics (Cat. No.98CH36132)*. IEEE, pp. 345–348. [Online]. Available: http://ieeexplore.ieee.org/document/709296/

[8] "Plastics-the Facts 2017 An analysis of European plastics production, demand and waste data," Tech. Rep. [Online]. Available: https://www.plasticseurope.org/application/files/5715/1717/4180/Plastics_the_facts_2017_FINAL_for_website_one_page.pdf

[9] N. G. McCrum, C. P. Buckley, and C. B. Bucknall, *Principles of polymer engineering*. Oxford University Press, 1997.

[10] F. Zhou, J. Li, Z. Yan, X. Zhang, Y. Yang, M. Liu, D. Min, and S. Li, "Investigation of charge trapping and detrapping dynamics in LDPE, HDPE and XLPE," *IEEE Transactions on Dielectrics and Electrical Insulation*, vol. 23, no. 6, pp. 3742–3751, 12 2016.

[11] L. A. Dissado and J. C. Fothergill, *Electrical Degradation and Breakdown in Polymers*. The Institution of Engineering and Technology, Michael Faraday House, Six Hills Way, Stevenage SG1 2AY, UK: IET, 1 1992.

[12] C. C. Ku and R. Liepens, *Electrical Properties of Polymers - Chemical Principles*. Münich: Carl Hanser Verlag, 1987.

[13] B. Lee, "Electrical conductivity of carbon black filled polymers—effects of morphology and processing," *Journal of Vinyl Technology*, vol. 15, no. 3, pp. 173–176, 1993.

[14] U. Nilsson and J.-O. Bostrom, "Influence of the semiconductive material on space charge build-up in extruded HVDC cables," in *2010 IEEE International Symposium on Electrical Insulation*. IEEE, 6 2010, pp. 1–4.

[15] Mitsubishi, "Manufacturing Process of Carbon Black." [Online]. Available: http://www.carbonblack.jp/en/cb/seizou.html?fbclid=IwAR0w4YsJGqGW1NeiYMNX0-I9WoqR7BlS9MSaMkxEufID8PjWlAqxbOb1hyM

[16] K. Jeppson, *Kurshäfte i Mikroelektronik*, Gothenburg, 2012.

[17] P. Morshuis, "Interfaces: To be avoided or to be treasured? What do we think we know?" in *2013 IEEE International Conference on Solid Dielectrics (ICSD)*. IEEE, 6 2013, pp. 1–9. [Online]. Available: http://ieeexplore.ieee.org/document/6619726/

[18] G. Chen, T. Tay, A. Davies, Y. Tanaka, and T. Takada, "Electrodes and charge injection in low-density polyethylene using the pulsed electroacoustic technique," *IEEE Transactions on Dielectrics and Electrical Insulation*, vol. 8, no. 6, pp. 867–873, 2001. [Online]. Available: http://ieeexplore.ieee.org/document/971439/

[19] G. Teyssedre and C. Laurent, "Charge transport modeling in insulating polymers: from molecular to macroscopic scale," *IEEE Transactions on Dielectrics and Electrical Insulation*, vol. 12, no. 5, pp. 857–875, 10 2005. [Online]. Available: http://ieeexplore.ieee.org/document/1522182/

[20] X. Liu and D. W. Schubert, "Influence of the pressure-dependent contact area between electrode and composite surface on the electrical conductivity," *Composite Structures*, vol. 136, pp. 414–418, 2 2016.

[21] Y. Mamunya, H. Zois, L. Apekis, and E. Lebedev, "Influence of pressure on the electrical conductivity of metal powders used as fillers in polymer composites," *Powder Technology*, vol. 140, no. 1-2, pp. 49–55, 2 2004. [Online]. Available: https://www.sciencedirect.com/science/article/pii/S0032591004000270

[22] D. Ketenoğlu and B. Ünal, "Influence of surface roughness on the electrical conductivity of semiconducting thin films," *Physica A: Statistical Mechanics and its Applications*, vol. 392, no. 14, pp. 3008–3017, 7 2013. [Online]. Available: https://linkinghub.elsevier.com/retrieve/pii/S0378437113002100

[23] KEYENCE, "Sa (Arithmetical Mean Height)." [Online]. Available: https://www.keyence.com/ss/products/microscope/roughness/surface/parameters.jsp

[24] ——, "Sq (Root Mean Square Height)." [Online]. Available: https://www.keyence.com/ss/products/microscope/roughness/surface/sq-root-mean-square-height.jsp

[25] Michigan Metrology, "3D S Height (Amplitude) Parameters: Sa (Average Surface Roughness) and Sq (RMS Surface Roughness)." [Online]. Available: https://www.michmet.com/3d_s_height_parameters_sasq.htm

[26] ——, "3D S Hybrid Parameters: Sdq (RMS Surface Slope)." [Online]. Available: https://www.michmet.com/3d_s_hybrid_parameters_sdq.htm

[27] H. Ghorbani, M. Saltzer, and C.-O. Olsson, "Observation of non-monotonic dependence of leakage current with temperature during thermal cycling," in *2016 IEEE Electrical Insulation Conference (EIC)*. IEEE, 6 2016, pp. 488–491.

[28] Advantech, "ADAM-4022T Serial Base Dual Loops PID Controller User's Manual," Tech. Rep. [Online]. Available: https://www.prosoft.ru/cms/f/261491/ADAM-4022Tpdf.pdf

[29] "Instruction Manual EW series," Glassman High Voltage Inc., Tech. Rep., 1996.

[30] H. Ghorbani, *Characterization of Conduction and Polarization Properties of HVDC Cable XLPE Insulation Materials*. KTH Royal Institute of Technology, 2018.

A

Appendix I

In section 4.3 the average thickness of the samples are presented and in Figure 4.6 an example of a cable peeling and its varying thickness can be observed. In Figure A.1 - A.5 the results from the microscope measurements on the cable peelings are shown.

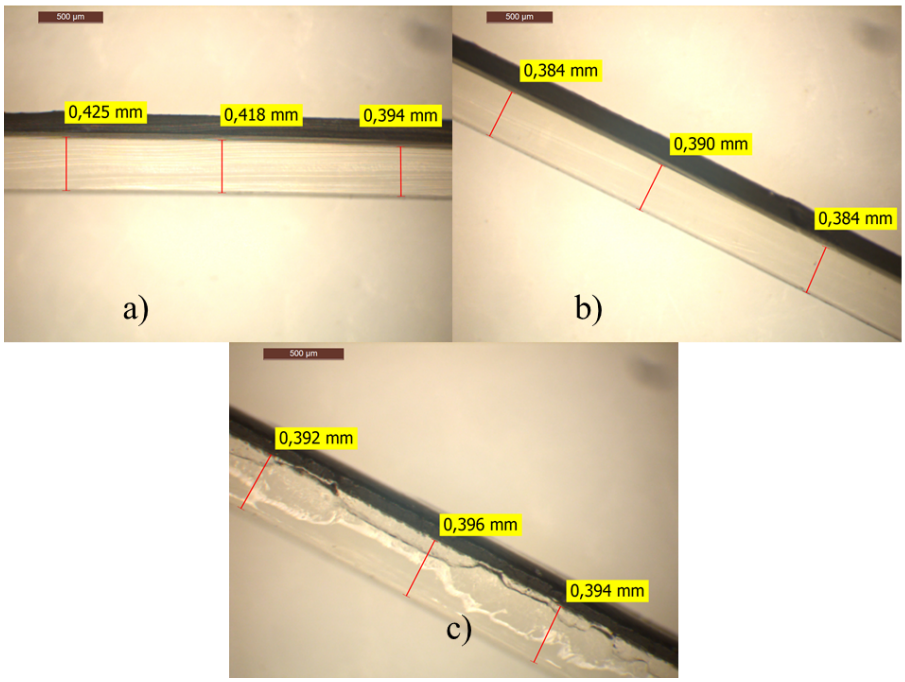

Figure A.1: Thickness of three different samples from cable peeling O08.

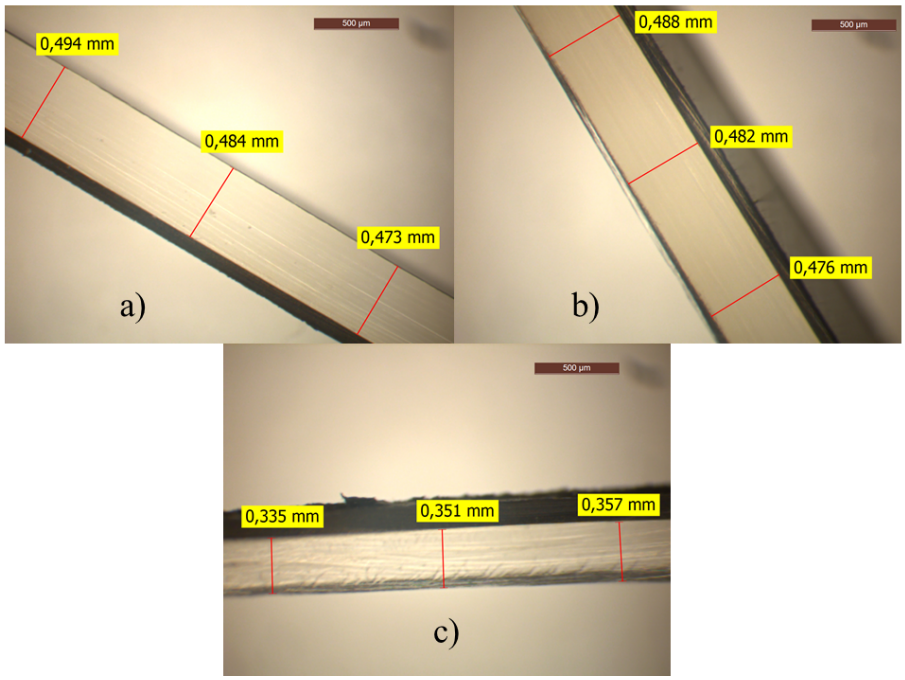

Figure A.2: Thickness of three different samples from cable peeling O10.

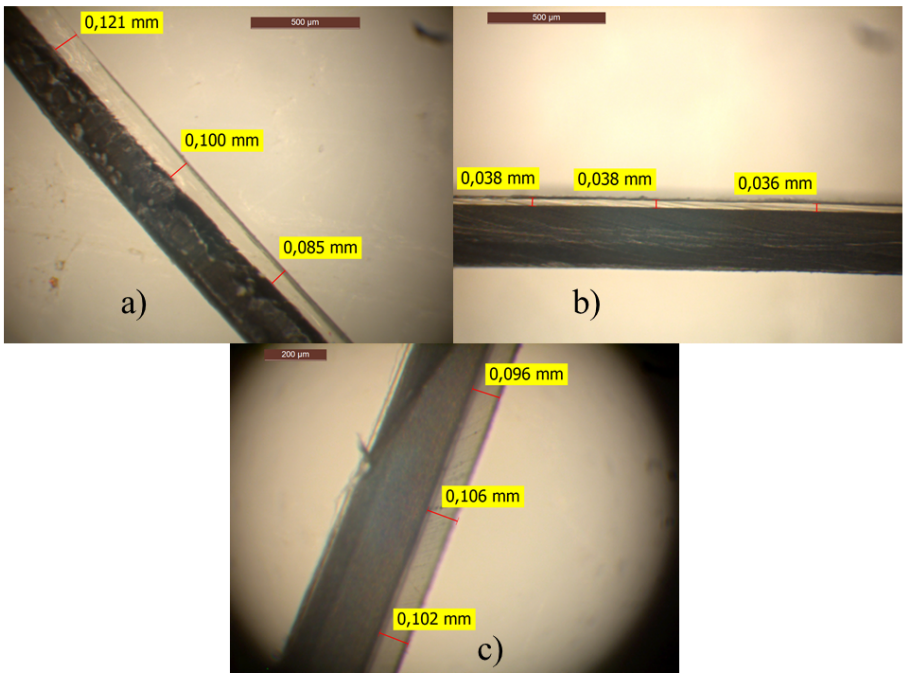

Figure A.3: Thickness of three different samples from cable peeling O11.

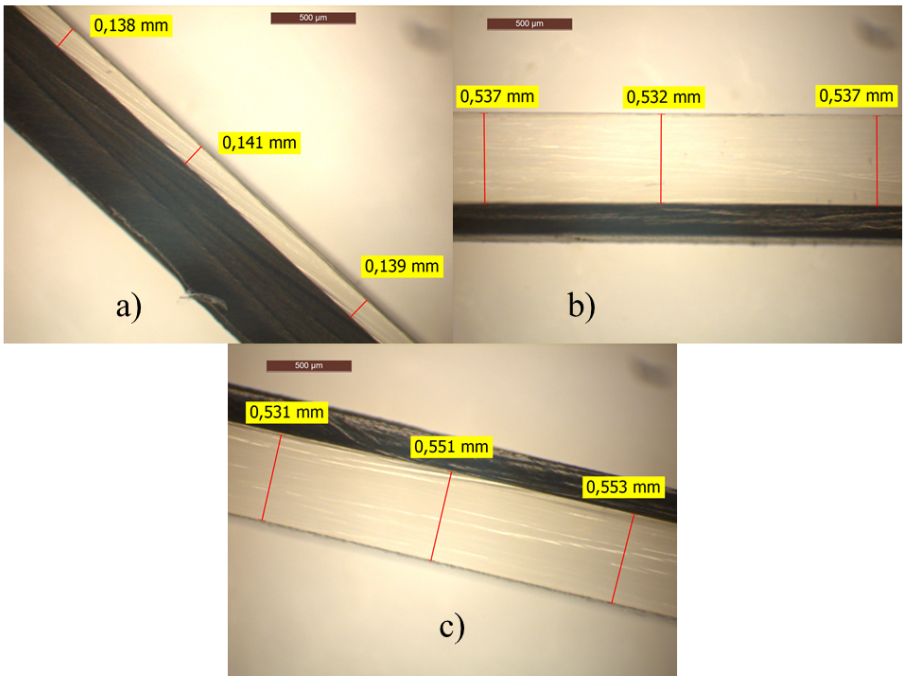

Figure A.4: Thickness of three different samples from cable peeling O14.

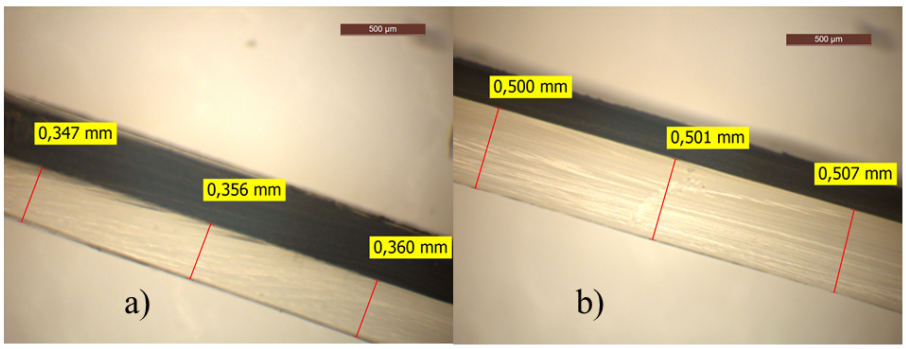

Figure A.5: Thickness of two different samples from cable peeling O15.